Ain Shams Engineering Journal (2016) 7, 313–333

Ain Shams University

Ain Shams Engineering Journal

www.elsevier.com/locate/asej
www.sciencedirect.com

MECHANICAL ENGINEERING

A homogenization procedure for geometrically non-linear free vibration analysis of functionally graded annular plates with porosities, resting on elastic foundations

Lhoucine Boutahar [a,*], **Khalid El bikri** [a,1], **Rhali Benamar** [b]

[a] *Université Mohammed V, Ecole Normale Supérieure de l'Enseignement Technique de Rabat, Département de génie mécanique, LaMIPI, B.P. 6207, Rabat Instituts, 10100 Rabat, Morocco*
[b] *Université Mohammed V, Ecole Mohammadia d'Ingénieurs, LERSIM, Av. Ibn Sina, Rabat, Morocco*

Received 3 December 2014; revised 9 September 2015; accepted 16 November 2015
Available online 14 January 2016

KEYWORDS

Non-linear vibration;
Annular plate;
Functionally Graded Material (FGM);
Porosities;
Homogenization procedure;
Elastic foundations

Abstract Some Functionally Graded Materials contain pores due to the result of processing; this influences their elastic and mechanical properties. Therefore, it may be very useful to examine the vibration behavior of thin Functionally Graded Annular Plates Clamped at both edges including porosities. In the present study, the rule of mixture is modified to take into account the effect of porosity and to approximate the material properties assumed to be graded in the thickness direction of the examined annular plate. A semi-analytical model based on Hamilton's principle and spectral analysis is adopted using a homogenization procedure to reduce the problem under consideration to that of an equivalent isotropic homogeneous annular plate. The problem is solved by a numerical iterative method. The effects of porosity, material property, and elastic foundations characteristics on the CCFGAP axisymmetric large deflection response are presented and discussed in detail.

1. Introduction

A lot of research and development have been carried out to investigate Functionally Graded Materials FGMs for various applications using gradients in physical, chemical, biochemical, and mechanical properties. The main characteristic that distinguishes FGMs from conventional composite materials is the possibility of tailoring the graded composition and microstructure in an intentional manner, destined to achieve the desired function. The design of FGM structures is based on an attempt to take the best benefit from the integration of the functions of

* Corresponding author. Tel.: +212 610738446.
E-mail addresses: lhoucineboutahar@gmail.com (L. Boutahar), k.elbikri@um5s.net.ma (K. El bikri), rbenamar@emi.ac.ma (R. Benamar).
[1] Tel.: +212 610738446.

Peer review under responsibility of Ain Shams University.

Production and hosting by Elsevier

http://dx.doi.org/10.1016/j.asej.2015.11.016
2090-4479

Nomenclature

CCFGAP Clamped–Clamped Functionally Graded Annular Plates
DQM, DSC Differential Quadrature Method and Discrete Singular Convolution respectively
HDQ, FEM Harmonic Differential Quadrature and Finite Element Method respectively
FSDT, FD First order Shear Deformation Theory and Finite Differences respectively
b, a, h inner radius, outer radius and thickness of the annular plate respectively
α inner to outer radius ratio of the annular plate. $\alpha = b/a$
λ thickness to outer radius ratio of the annular plate. $\lambda = h/a$
ϑ_c, ϑ_m volume fraction of ceramic and metal respectively
k, ζ gradient index and porosity volume fraction respectively
ν Poisson's ratio of the annular plate material
E_c, E_m Young's modulus of ceramic and metal respectively
ρ_c, ρ_m mass density of ceramic and metal respectively
(r, θ, z) cylindrical co-ordinates
W, U transverse and in-plane displacements of the middle plane point (r, θ, z) respectively
u_r, u_z displacements along r and z directions respectively
$\varepsilon_r, \varepsilon_\theta$ radial and circumferential strains respectively
V_b, V_m, V bending, membrane and total strain energy respectively
V_f, T potential energy of the elastic foundation and Kinetic energy
K_L, K_{NL}, K_S Winkler, non-linear and shear layer foundation parameters respectively
A_{11}, B_{11}, D_{11} extensional stiffness, extensional–bending coupling stiffness and bending stiffness respectively
δ, β, γ $\delta = B_{11}/A_{11}, \beta = \left(A_{11}h^2\right)/\overline{D_{11}}, \gamma = \left(A_{11}h^2\right)/4\overline{D_{11}}$
Mode (m, n) m: nodal diameters. n: interior nodal circles
$k_{ij}^w, m_{ij}^w, b_{ijkl}^w$ general terms of the rigidity tensor, the mass tensor and the fourth order non-linearity tensor, respectively, associated with the transverse displacement
k_{ij}^u, m_{ij}^u general terms of the rigidity tensor and the mass tensor, respectively, associated with the in-plane displacement
C_{ijk}^{uw} general term of the third order non-linearity rigidity tensor representing the coupling between the in- and the transverse displacements
d_{ijk}^* general term of the third order tensor allowing the calculation of the kth in-plane contribution coefficient
b_{ijkr}^* general term of the fourth order non-linearity rigidity tensor taking into account the influence of the in-plane displacement
w_{max}^* maximum non-dimensional vibration amplitude
$w(r)$ transverse shape function $W(r,t) = w(r)\cos(\omega t)$
$u(r)$ in-plane shape function $U(r,t) = u(r)cos^2(\omega t)$
a_i, b_i contribution coefficient of the ith transverse and in-plane basic function respectively. $w(r) = a_i w_i(r), u(r) = b_i u_i(r)$
po, pi number of transverse and in-plane basic functions respectively
$\{A\}$ column matrix of transverse contribution coefficients: $\{A\}^T = \left[a_1, a_2, \ldots, a_{po}\right]$
η_i the ith transverse eigenvalue parameter for axisymmetric CCFGAP
ξ_i the ith in-plane eigenvalue parameter for axisymmetric CCFGAP
$\left(\omega_{nl}^*/\omega_l^*\right)_i$ the ith non-dimensional frequency ratio
$\sigma_{br}, \sigma_{b\theta}$ radial and circumferential bending stresses
$\sigma_{mr}, \sigma_{m\theta},$ radial and circumferential membrane stresses
σ_{tr} radial total stress
* star exponent indicates non-dimensional parameter

refractoriness, high wear resistance hardness, thermal shock resistance, and corrosion resistance of ceramics on the one hand as well as the high strength and toughness of metals on the other hand. This has led to a variety of structural applications [1]. FGMs that are made from a mixture of metal and ceramics are typically characterized by a smooth and continuous change of the mechanical, physical, and chemical properties from one side to the other [2–4]. These FGMs designs are reported to overcome weaknesses of laminated composite materials such as de-bonding under massive stress, local large plastic deformations or the buildup of residual stresses caused by the large difference in thermal expansion coefficients among components [5]. Generally speaking, the compositional gradient obtained in FGMs offers an excellent solution for such cases as a result of a continuous transition from one material property to the other avoiding abrupt mismatch [6], which keeps the thermo-mechanical stresses within acceptable limits and minimizes the residual thermal stresses [7]. FGMs have been widely used in aerospace, energy, electronics, and other industries. With the increasing attention of researchers, a wide variety of processes has been used in the preparation of FGMs such as powder metallurgy, vapor deposition, self-propagation, centrifugal casting, and magnetic separation [8–12]. All of these methods mentioned above have their own drawbacks such as high costs and complexity of the technique. The sintering process proves to be a flexible and suitable route for FGM manufacturing. However, during the process, microvoids or porosities can occur within the material, due to the large difference in the solidification temperatures between the material constituents [13]. The presence of small pores results in a sharp decrease in strength and elastic modulus. Hence, it is important to take into account the porosity effect when designing FGM structures subjected to dynamic loadings. To describe the interaction of a plate with its foundation, various basic models have

been proposed in the literature. The simplest model for the elastic foundation is Winkler model, which considers the foundation as a set of separate and independent springs. This was later improved by Pasternak which takes into account the interactions between the separated springs in Winkler model by introducing a new dependence parameter. Plates resting on elastic foundations have been widely adopted by many researchers to model interaction between elastic media and plates for various engineering problems. There are some research studies on the free vibration of beams, rectangular, circular and annular plates resting on elastic foundations. Ying et al. [14] presented Two-dimensional elasticity solutions for functionally graded beams on elastic foundations. Pradhan and Murmu [15] analyzed thermo-mechanical vibration of FGM sandwich beam under variable elastic foundations by DQM. Malekzadeh [16] studied 3-D free vibration of thick functionally graded plates on elastic foundations. Huang et al. [17] presented Benchmark solutions for functionally graded thick plates resting on Winkler–Pasternak elastic foundations. Civalek and Akgöz [18] used DSC method for non-linear analysis of laminated plates resting on Winkler–Pasternak elastic foundations. Civalek investigated geometrically non-linear static and dynamic analysis of thin rectangular plates resting on Winkler–Pasternak elastic foundations, using [19] DSC-HDQ coupled methodology and [20] HDQ-FD coupled methodology. Dumir et al. [21] investigated geometrically non-linear axisymmetric vibration of orthotropic thin circular plates on elastic foundations using an orthogonal point collocation method for spatial discretization and Kantorovich averaging method to eliminate the time t. Zhou et al. [22] presented 3-D free vibration of thick circular plates on Pasternak foundation. Hosseini Hashemi et al. [23] investigated 3-D free vibration analysis of annular plates on Pasternak elastic foundation by p-Ritz method. Malekzadeh et al. [24] investigated the free vibration analysis of FG thin-to-moderately thick annular plates subjected to thermal environment on elastic foundation based on the FSDT using DQM. However, the vibration analyses of structures with porosities resting on elastic foundations are rather rare and the available results are limited to FG beams with porosities [25]. Thin plates made of Functionally Graded Materials with or without an elastic foundation have found wide applications as a component in practical engineering structures such as aerospace, marine industry, biomechanics, petrochemical, mechanical and civil engineering, nuclear engineering, and reactors. There are many situations such as seismic tests, nuclear explosions, and earthquakes, in which these structures are subjected to transient loads and where large amplitudes of motion may occur, sometimes exceeding the plate thickness. Therefore, a dynamic analysis of such components taking into account the geometric nonlinearity is important for the safety and stability of the structures. In this case, the linear models are not sufficient to predict the behavior of the plates. Geometrically non-linear vibration of some structures, beams, plates and shells, with different boundary conditions has long been a subject receiving numerous research efforts, as evidenced by many analytical, semi-analytical and numerical studies reported in the open literature. For a good understanding of the progress in this field, interested readers may consult the reviews presented in [26–30]. Compared with the free vibration analysis of FG beams and rectangular plates (see for example [31–42]), the studies concerned FG circular and annular plates are very limited in number, and are briefly discussed below. Reddy et al. [43] investigated the axisymmetric bending of FG circular and annular plates using the FSDT to formulate the problem. Gunes and Reddy [44] used the Green–Lagrange strain tensor to analyze the geometrically non-linear vibration of FG circular plates subjected to mechanical and thermal loads, and a homogenization method based on the Mori–Tanaka scheme to evaluate material properties. Ma and Wang [45] analyzed the non-linear bending and post-buckling of a FG circular plate under mechanical and thermal loadings. Prakash and Ganapathi [46] analyzed the asymmetric free vibration characteristics and thermoelastic stability of FG circular plates based on the FSDT using the FEM. Eraslan and Akis [47] obtained the closed-form solution for FG rotating solid shaft and rotating solid disk under generalized plane strain and plane stress assumptions, respectively. Efraim and Eisenberger [48] achieved the exact vibration analysis of thick annular isotropic and functionally graded plates with a variable thickness using the FSDT to formulate the problem. Nie and Zhong [49] investigated the three-dimensional vibration of functionally graded circular plates using a semi-analytical method based on the state space method and DQM. Dong [50] studied the three-dimensional free vibration of FG circular and annular plates using the Chebyshev–Ritz method. Nie and Zhong [51] used a semi-analytical numerical method based on the state space and DQM to study the dynamic behavior of multi-directional FG annular plates. Chakraverty et al. [52] presented the effect of non-homogeneity of the material properties on the vibration frequencies of circular and elliptic plates. They used boundary characteristic orthogonal polynomials as the basis function in the Rayleigh Ritz method to solve the problem. A model based on Hamilton's principle and spectral analysis has been developed in the previous series of works [53–69] for non-linear free vibrations of thin straight structures, such as beams, plates, and shells. In this model, the non-linear free vibration problem is reduced to a set of non-linear algebraic equations suggested as a problem solution that has been numerically performed using appropriate algorithms in order to obtain a set of non-linear mode shapes for the structure considered in each case, with the corresponding amplitude dependent non-linear frequencies. The main features of this approach have been discussed for the first time in [53]. However, although the works mentioned above made it quite easy to calculate the non-linear mode shapes, the non-linear frequencies and the non-linear stresses of the structures considered, via numerical solution of a small set of non-linear algebraic Eqs. ((5) for beams [54], 6 for clamped circular plates [68], 8 for fully clamped rectangular plates [55], 11 for shells [57]), it was thought that further investigations could be directed toward a further step in the development of a sort of non-linear modal analysis theory. This should allow easy calculation of the non-linear free response of thin straight structures, in terms of their classical mass and rigidity matrices, the non-linear geometrical rigidity tensor introduced in the above model, and the amplitude of vibration. The accuracy of the method, which can be considered as an extension of the Rayleigh–Ritz method to non-linear vibrations, will be mainly influenced by the choice of the admissible functions, defined by Amabili and Garziera [70] as the eigenfunctions of the closest simple problem extracted from the considered one.

The objective of the present work was to determine the geometrically non-linear free vibration response of CCFGAP with

porosities resting on various elastic foundations, using the theoretical model discussed above. The displacements of a given point of the middle plane of the plate are expanded in the form of finite series of admissible functions, which satisfy the boundary conditions. Upon assuming harmonic motion, the discretized expressions for the total strain and kinetic energies of the plate are then derived, and by applying Hamilton's principle, and integrating the time functions over the range $[0, \pi/(2\omega)]$ to eliminate the time t, the problem is reduced to a system of coupled non-linear algebraic equations. These amplitude equations may be decoupled, by neglecting the in plane inertia. The solution is then obtained numerically using an iterative procedure described in [71–73] for fully clamped isotropic and laminated rectangular plates. The work is restricted for consideration of the fundamental axisymmetric mode in order to concentrate on the study of the influence of the material property distribution, the porosity, and the elastic foundation parameters on the plate non-linear dynamic response near to the fundamental resonance.

2. General formulation

2.1. Problem definition

Consider the thin functionally graded annular plate clamped at both edges (CCFGAP), of uniform thickness (h), outer radius (a) and inner radius (b). It is made of a mixture of ceramic and metal whose compositions vary from the top to the bottom surface. The top surface ($z = +h/2$) of the plate is ceramic-rich whereas the bottom surface ($z = -h/2$) is metal-rich. In this investigation, the imperfect CCFGAP is assumed to have porosities spreading within the plate cross section due to a defect during production. CCFGAP's geometry and its cross-sectional area including porosity phases are shown in Fig. 1. The numerical results presented in this paper correspond to the thickness ($h = 0,01$), the outer and inner radius ($a = 0,5, b = 0,05$), and the inner to outer radius ratio ($\alpha = b/a = 0.1$).

2.2. Mechanical properties of the FGAP with porosities

The material property P (e.g., Young's modulus E, mass density ρ and Poisson's ratio v) of the FGAP with porosities examined here is assumed to vary through the thickness of the plate, as a function of the volume fraction, the properties of the constituent materials, and the porosity volume fraction $\zeta(\zeta \ll 1)$. Two kinds of porosity distribution through the plate thickness among the metal and ceramic are considered in this study, following the choice made in [25].

The porosity in the first scenario is even among the metal and ceramic. The modified rule of mixture is proposed as follows:

$$P(z) = P_m\left(\vartheta_m - \frac{\zeta}{2}\right) + P_c\left(\vartheta_c - \frac{\zeta}{2}\right) \tag{1}$$

In which ϑ_c and ϑ_m are the ceramic and metal volume fractions, respectively and are related by the following:

$$\vartheta_m + \vartheta_c = 1 \tag{2}$$

and the power law of volume fraction of the ceramic ϑ_c is defined by [74]:

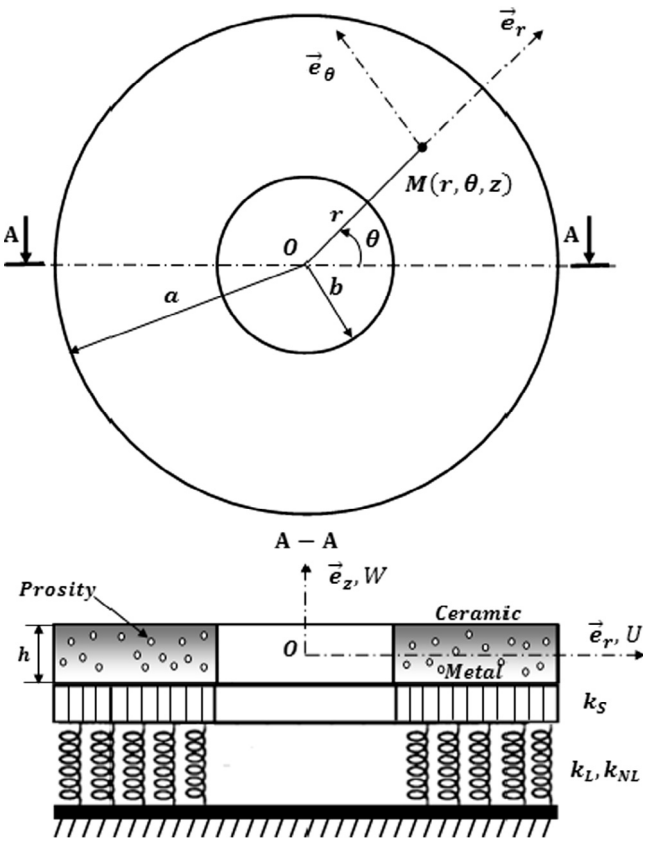

Figure 1 Geometry and coordinate system of CCFGAP with porosities, resting on elastic foundations.

$$\vartheta_c(z) = \left(\frac{z}{h} + \frac{1}{2}\right)^k, \quad k \geqslant 0 \tag{3}$$

The gradient index (k) dictates the material variation profile across the plate thickness. It is assumed that the effective Young's modulus (E) and the mass density (ρ) vary along the plate thickness while the Poisson's ratio (v) is considered to be constant.

Hence, all properties of the imperfect FGAP can be written as follows:

$$P(z) = (P_c - P_m)\left(\frac{z}{h} + \frac{1}{2}\right)^k + P_m - (P_c + P_m)\frac{\zeta}{2} \tag{4}$$

Eq. (4) shows that if ($k = 0$), the plate reduces to a pure ceramic plate. As the gradient index increases, the ceramic volume fraction decreases until it is small enough such that the material properties tend to pure metal. The material properties of a perfect FGAP can be obtained when (ζ) is set to zero. Thus, Young's modulus (E) and material density (ρ) expressions of the imperfect CCFGAP can be formulated as follows:

$$E(z) = (E_c - E_m)\left(\frac{z}{h} + \frac{1}{2}\right)^k + E_m - \frac{\zeta}{2}(E_c + E_m) \tag{5}$$

$$\rho(z) = (\rho_c - \rho_m)\left(\frac{z}{h} + \frac{1}{2}\right)^k + \rho_m - \frac{\zeta}{2}(\rho_c + \rho_m) \tag{6}$$

In the second scenario, the porosities are distributed around the middle zone of the cross section, and the amount of porosity decreases and tends to zero at the top and bottom of the

Table 1 Material property of metal and ceramic constituents of the FGAP.

Materials	Young's modulus E (GPa)	Poisson's ratio υ
Ceramic (Zirconia)	110.25	0.288
Metal (Aluminum)	278.41	0.288

cross section. Based on the principle of the multi-step sequential infiltration technique that can be used to produce FGM samples, the porosities mostly occur at the middle zone [75]. In this zone, it is difficult to infiltrate the materials completely while at the top and bottom zones and the process of material infiltration can easily be performed. It can also lead to less porosity. The expressions for Young's modulus (E) and the material density (ρ) in Eqs. (5) and (6) are modified as follows:

$$E(z) = (E_c - E_m)\left(\frac{z}{h}+\frac{1}{2}\right)^k + E_m - \frac{\zeta}{2}(E_c + E_m)\left(1 - \frac{2|z|}{h}\right) \tag{7}$$

$$\rho(z) = (\rho_c - \rho_m)\left(\frac{z}{h}+\frac{1}{2}\right)^k + \rho_m - \frac{\zeta}{2}(\rho_c + \rho_m)\left(1 - \frac{2|z|}{h}\right) \tag{8}$$

All of the material properties used in the present study are taken from Reddy et al. [76] and summarized in Table 1.

Young's modulus variations through the plate thickness adopted here are illustrated in Fig. 2(a)–(d). As it can be seen in Fig. 2(a), in which the variation of Young's modulus through the plate thickness without porosities is presented, the material composition is continuously varying in such a manner that the top surface ($z/h = +0.5$) of the plate is ceramic rich, whereas the bottom surface ($z/h = -0.5$) is metal rich. In Fig. 2(b) and (c), two variations of Young's modulus through the plate thickness corresponding to two kinds of porosity distribution are presented. In Fig. 2(b), in which the porosities are spreading within the plate cross section, one observes the same form of curves more than those obtained in Fig. 2(a), with a decrease in Young's modulus, leading to a decrease in the plate stiffness through the whole plate cross section. In Fig. 2(c), the porosities are spreading around the middle zone of the cross section, and the amount of porosity tends to zero at the top and bottom of the cross section. The maximum of Young's modulus is reached at the top and bottom of the cross section and decreases in the direction of the middle zone, leading to a low stiffness around the plate mid-plane. Fig. 2(d) shows that the second kind of porosity distribution exhibits a less decrease in the plate stiffness than the first kind does, except at the neutral surface where it is the

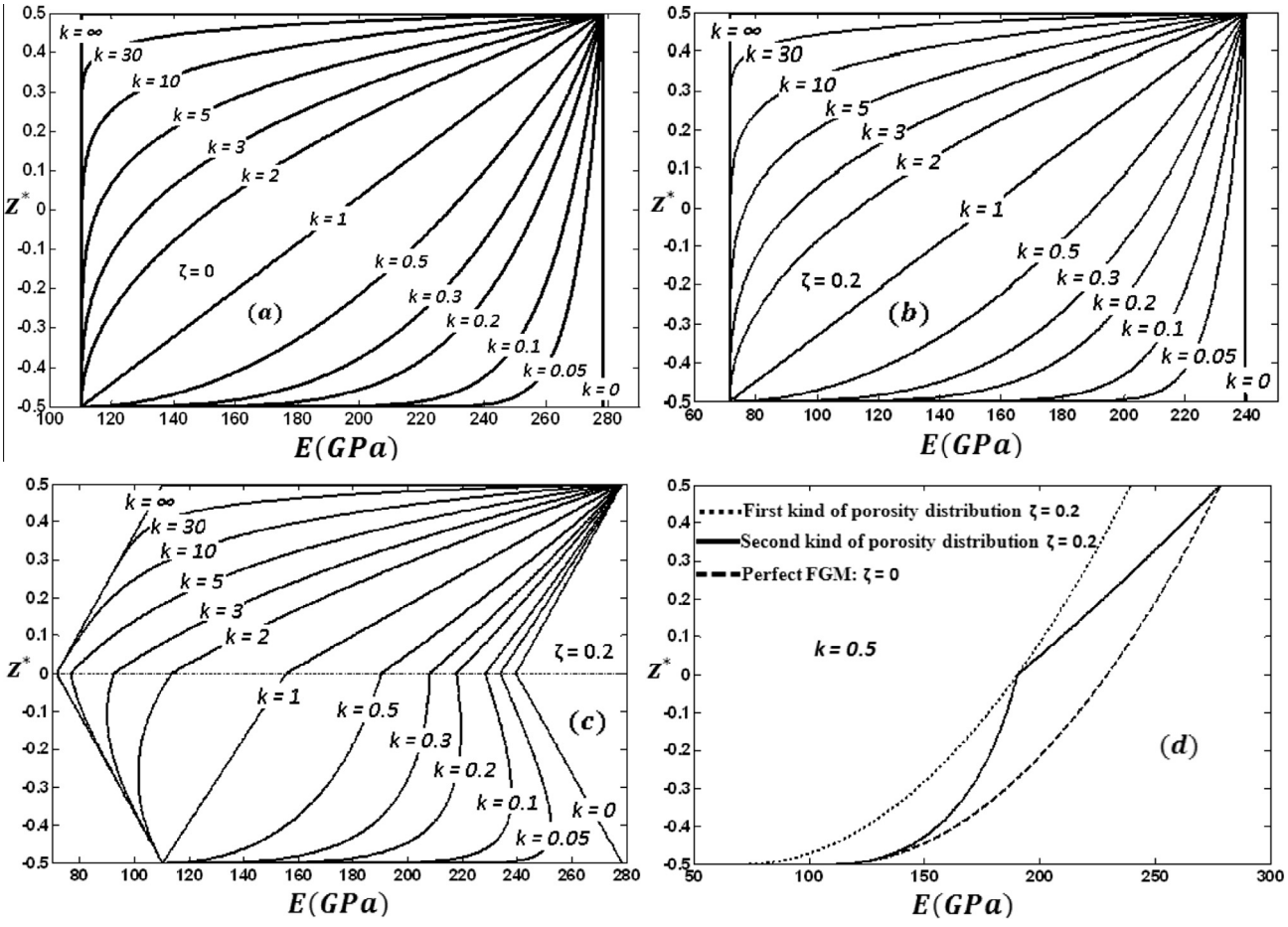

Figure 2 Variation of Young's modulus through the plate thickness for different values of gradient index: (a) Perfect FGM, (b) first kind of porosity distribution, (c) second kind of porosity distribution, and (d) comparison of the two kinds of porosity distribution.

same. The variation of Young's modulus through thickness of the imperfect FGAP with the first and second kind of porosity distribution is plotted in Fig. 3(a) and (b) respectively, for different values of the porosity volume fraction. These figures show that Young's modulus decreases with increasing the porosity volume fraction. The decrease of Young's modulus indicates a decrease in the plate stiffness.

2.3. Basic theory

2.3.1. Displacement field of the annular plate

According to the Classical Plate Theory (CPT), the displacement field of an annular plate in the cylindrical coordinates system is given by [77]:

$$u_r(r,z,t) = U(r,t) - z\frac{\partial W(r,t)}{\partial r} \tag{9}$$

$$u_z(r,t) = W(r,t) \tag{10}$$

where u_z and u_r are the displacements in the transverse z-direction and radial r-direction of the plate, respectively; $W(r,t)$ is the transverse displacement and $U(r,t)$ is the radial displacement of the mid-plane. The strains for a thin annular plate at any level z are obtained by using the geometric non-linear theory of thin plates in a Von Karman's sense, leading to the following:

$$\varepsilon_r = \frac{\partial U}{\partial r} + \frac{1}{2}\left(\frac{\partial W}{\partial r}\right)^2 - z\frac{\partial^2 W}{\partial r^2} \tag{11}$$

$$\varepsilon_\theta = \frac{U}{r} - \frac{z}{r}\frac{\partial W}{\partial r} \tag{12}$$

2.3.2. Total strain and kinetic energy expressions of FGAP

The total strain energy, V, of the annular plate is given as the sum of the strain energy due to the bending V_b, the membrane strain energy due to the non-linear stretching forces induced by large deflections V_m and the potential energy of the elastic foundation V_f.

$$V = V_b + V_m + V_f \tag{13}$$

The expressions used for, V_b, V_m, V_f and the kinetic energy T depend on the considered problem as well as the adopted hypotheses.

$$V_b = \pi\int_b^a \left(D_{11}\left[\left(\frac{\partial^2 W}{\partial r^2}\right)^2 + \frac{1}{r^2}\left(\frac{\partial W}{\partial r}\right)^2 + \frac{2\nu}{r}\frac{\partial W}{\partial r}\frac{\partial^2 W}{\partial r^2}\right] - B_{11}\left[\left(\frac{\partial W}{\partial r}\right)^2\frac{\partial^2 W}{\partial r^2} + \frac{\nu}{r}\frac{\partial W}{\partial r}\left(\frac{\partial W}{\partial r}\right)^2\right]\right) r\,dr \tag{14}$$

$$V_m = \pi A_{11}\int_b^a \left[\left(\frac{\partial U}{\partial r}\right)^2 + \frac{\partial U}{\partial r}\left(\frac{\partial W}{\partial r}\right)^2 + \frac{1}{4}\left(\frac{\partial W}{\partial r}\right)^4 + \frac{U^2}{r^2} + \frac{2\nu U}{r}\frac{\partial U}{\partial r} + \frac{\nu U}{r}\left(\frac{\partial W}{\partial r}\right)^2\right] r\,dr - 2\pi B_{11}\int_b^a \left[\frac{\partial U}{\partial r}\frac{\partial^2 W}{\partial r^2} + \frac{U}{r^2}\frac{\partial W}{\partial r} + \frac{\nu}{r}\frac{\partial U}{\partial r}\frac{\partial W}{\partial r} + \frac{\nu U}{r}\frac{\partial^2 W}{\partial r^2}\right] r\,dr \tag{15}$$

where

$$(A_{11}, B_{11}, D_{11}) = \int_{-h/2}^{h/2}\frac{E(z)}{1-\nu^2}(1, z, z^2)\,dz \tag{16}$$

The extensional stiffness A_{11}, extensional–bending coupling stiffness B_{11} and bending stiffness D_{11} of FGAP can be written as functions of the gradient index (k) as follows:

$$A_{11} = \frac{h}{(1-\nu^2)}\left[\frac{(E_c - E_m)}{(k+1)} + E_m - \frac{\zeta}{2}(E_c + E_m)\right] \tag{17}$$

$$B_{11} = \frac{(E_c - E_m)h^2}{(1-\nu^2)}\left[\frac{k}{2(k+1)(k+2)}\right] \tag{18}$$

$$D_{11} = \frac{h^3}{(1-\nu^2)}\left[\frac{(E_c - E_m)(k^2+k+2)}{4(k+1)(k+2)(k+3)} + \frac{E_m}{12} - \frac{\zeta}{24}(E_c + E_m)\right] \tag{19}$$

$$V_f = \pi K_L\int_b^a W^2 r\,dr + \frac{\pi}{2}K_{NL}\int_b^a W^4 r\,dr + \pi K_S\int_b^a \left(\frac{\partial W}{\partial r}\right)^2 r\,dr \tag{20}$$

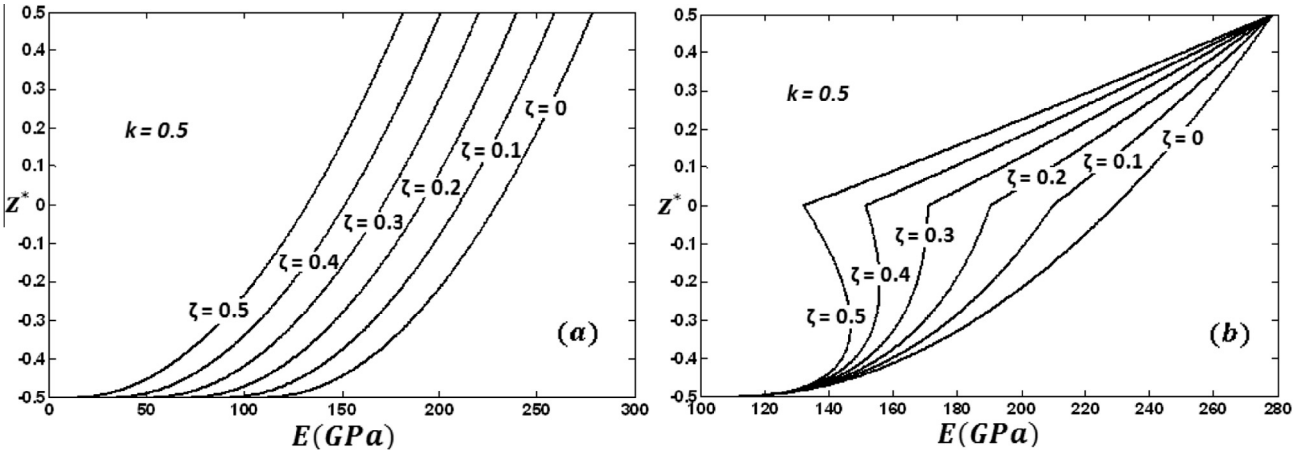

Figure 3 Effects of the porosity volume fraction on Young's modulus of the imperfect CCFGAP: (a) first kind of porosity distribution and (b) second kind of porosity distribution.

where K_L, K_{NL}, K_S are the Winkler, non-linear and shear layer foundation parameters respectively.

In most engineering applications of thin plates, rotatory and in-plane inertia effects can be neglected [78]. Thus, the kinetic energy of an annular plate reduces to the following:

$$T = \pi I_0 \int_b^a \left[\left(\frac{\partial W}{\partial t}\right)^2 + \left(\frac{\partial U}{\partial t}\right)^2 \right] r\, dr, \quad I_0 = \int_{-h/2}^{h/2} \rho(z) dz \tag{21,22}$$

and ρ is the mass per unit volume of the plate material.

2.3.3. The homogenization procedure

Herein, a new coordinate system is assumed which is at the distance δ from the previous one [79,80], defined by:

$$z = \bar{z} + \delta \tag{23}$$

where δ is the vertical distance between the forgoing coordinate system and the new one. The new coordinate is applied and can be written as follows:

$$\begin{aligned} A_{11} &= \int_{-\frac{h}{2}}^{\frac{h}{2}} \frac{E(z)}{1-\nu^2} dz = \int_{-\frac{h}{2}}^{\frac{h}{2}} \frac{E(\bar{z})}{1-\nu^2} d\bar{z} \\ A_{11} &= \overline{A_{11}} \end{aligned} \tag{24a}$$

The effective extensional stiffness A_{11} does not change in this new coordinate system.

$$\begin{aligned} B_{11} &= \int_{-\frac{h}{2}}^{\frac{h}{2}} \frac{E(z)}{1-\nu^2} z dz \\ &= \int_{-\frac{h}{2}}^{\frac{h}{2}} \frac{E(\bar{z})}{1-\nu^2} \bar{z} d\bar{z} + \delta \int_{-\frac{h}{2}}^{\frac{h}{2}} \frac{E(\bar{z})}{1-\nu^2} d\bar{z} \\ B_{11} &= \overline{B_{11}} + \delta A_{11} \end{aligned} \tag{24b}$$

Now, we put $\delta = B_{11}/A_{11}$ in order to achieve $\overline{B_{11}} = 0$.

$$\begin{aligned} D_{11} &= \int_{-\frac{h}{2}}^{\frac{h}{2}} \frac{E(z)}{1-\nu^2} z^2 dz \\ &= \int_{-\frac{h}{2}}^{\frac{h}{2}} \frac{E(\bar{z})}{1-\nu^2} \bar{z}^2 d\bar{z} + 2\delta \int_{-\frac{h}{2}}^{\frac{h}{2}} \frac{E(\bar{z})}{1-\nu^2} \bar{z} d\bar{z} + \delta^2 \int_{-\frac{h}{2}}^{\frac{h}{2}} \frac{E(\bar{z})}{1-\nu^2} d\bar{z} \\ &= \overline{D_{11}} + 2\delta \overline{B_{11}} + \delta^2 A_{11} \\ \overline{D_{11}} &= D_{11} - B_{11}^2/A_{11} \end{aligned} \tag{24c}$$

where $\overline{D_{11}}$ is the effective bending stiffness.

As the vertical displacement in the new coordinate system is the same as in the previous one, Eqs. (14) and (15) in the new system can be converted to:

$$V_b = \pi \overline{D_{11}} \int_b^a \left[\left(\frac{\partial^2 W}{\partial r^2}\right)^2 + \frac{1}{r^2}\left(\frac{\partial W}{\partial r}\right)^2 + 2\frac{\nu}{r}\frac{\partial W}{\partial r}\frac{\partial^2 W}{\partial r^2} \right] r\, dr \tag{25}$$

$$V_m = \pi A_{11} \int_b^a \left[\left(\frac{\partial U}{\partial r}\right)^2 + \frac{\partial U}{\partial r}\left(\frac{\partial W}{\partial r}\right)^2 + \frac{1}{4}\left(\frac{\partial W}{\partial r}\right)^4 + \frac{U^2}{r^2} + \frac{2\nu U}{r}\frac{\partial U}{\partial r} + \frac{\nu U}{r}\left(\frac{\partial W}{\partial r}\right)^2 \right] r\, dr \tag{26}$$

2.3.4. Discretization of the total strain and kinetic energy expressions

The transverse displacement function $W(r,t)$, which is mainly concerned with the amplitude dependence of the first harmonic component spatial distribution, is given by:

$$W(r,t) = w(r)cos(\omega t) \tag{27}$$

The in-plane displacement function $U(r,t)$ is taken in the following form:

$$U(r,t) = u(r)cos^2(\omega t) \tag{28}$$

The spatial functions $w(r)$ and $u(r)$ are expanded in the form of finite series of p_o and p_i transverse $w_i(r)$ and in-plane $u_i(r)$ basic functions, respectively, as follows:

$$w(r) = a_i w_i(r), \quad u(r) = b_i u_i(r) \tag{29}$$

where the usual summation convention for repeated indices is used from 1 to po and from 1 to pi for the $a_i's$ and $b_i's$ coefficients respectively. The discretized forms for the total strain and kinetic energies are respectively given by the following:

$$\begin{aligned} V = &\frac{1}{2} a_i a_j k_{ij}^w cos^2(\omega t) \\ &+ \frac{1}{2}\left[a_i a_j a_k a_l b_{ijkl}^w + a_i a_j b_k C_{ijk}^{uw} + b_i b_j k_{ij}^u \right] cos^4(\omega t) \end{aligned} \tag{30}$$

$$T = \frac{1}{2}\omega^2 \left[a_i a_j m_{ij}^w sin^2(\omega t) + b_i b_j m_{ij}^u sin^2(2\omega t) \right] \tag{31}$$

In these equation $m_{ij}^w, m_{ij}^u, k_{ij}^w, k_{ij}^u$ s, are the mass and rigidity tensors associated with w and u, respectively, b_{ijkl}^w and C_{ijk}^{uw} are the fourth and third order non-linearity and coupling tensors respectively. The general terms of these tensors are given by:

$$m_{ij}^w = 2\pi I_0 \int_b^a w_i w_j r\, dr \tag{32}$$

$$m_{ij}^u = 2\pi I_0 \int_b^a u_i u_j r\, dr \tag{33}$$

$$\begin{aligned} k_{ij}^w = &2\pi \overline{D_{11}} \int_b^a \left(\frac{dw_i^2}{dr^2}\frac{dw_j^2}{dr^2} + \frac{1}{r^2}\frac{dw_i}{dr}\frac{dw_j}{dr} \right) r\, dr \\ &+ \pi K_L \int_b^a w_i w_j r\, dr + \pi K_S \int_b^a \frac{dw_i}{dr}\frac{dw_j}{dr} r\, dr \end{aligned} \tag{34}$$

$$k_{ij}^u = 2\pi A_{11} \int_b^a \left(\frac{du_i}{dr}\frac{du_j}{dr} + \frac{1}{r^2}u_i u_j + \frac{\nu}{r}\frac{du_i}{dr}u_j + \frac{\nu}{r}u_i\frac{du_j}{dr} \right) r\, dr \tag{35}$$

$$C_{ijk}^{uw} = 2\pi A_{11} \int_b^a \left(\frac{dw_i}{dr}\frac{dw_j}{dr}\frac{du_k}{dr} + \frac{\nu}{r}\frac{dw_i}{dr}\frac{dw_j}{dr}u_k \right) r\, dr \tag{36}$$

$$b_{ijkl}^w = \pi \frac{A_{11}}{2} \int_b^a \frac{dw_i}{dr}\frac{dw_j}{dr}\frac{dw_k}{dr}\frac{dw_l}{dr} r\, dr + \frac{\pi}{2} K_{NL} \int_b^a w_i w_j w_k w_l r\, dr \tag{37}$$

It appears from Eqs. (32)–(37) that the mass and rigidity tensors are symmetric, and that the fourth order tensor b_{ijkl}^w and the third order tensor C_{ijk}^{uw} are such:

$$b_{ijkl}^w = b_{klij}^w = b_{jilk}^w = b_{ikjl}^w, \quad C_{ijk}^{uw} = C_{jik}^{uw} \tag{38}$$

2.3.5. Governing equations

It is well known that the dynamic behavior for a conservative system may be obtained by the application of Hamilton's principle, which, if no forcing term is considered, can be written as follows:

$$\partial \int_0^{\frac{\pi}{2\omega}} (V - T)dt = 0 \tag{39}$$

Replacing T and V by their discretized expressions in the energy condition (39), integrating the time functions over the range $(0, 2\pi/\omega)$ and calculating the derivatives with respect to the $a_i's$ and $b_i's$, and taking into account the properties of symmetry of the tensors involved, lead to the following coupled two sets of non-linear algebraic equations:

Table 2 First six dimensionless linear frequency parameters of the perfect CCFGAP transverse axisymmetric vibration for various inner to outer radius ratios ($\zeta = 0$, $k = 0$).

Mode	b/a						
(m, n)	0.1	0.2	0.3	0.4	0.5	0.6	0.7
(0, 1)	27.2805	34.60850	45.34540	61.87080	89.2496	139.6179	248.3997
(0, 2)	75.3650	95.74040	125.3616	170.8981	246.3424	385.1524	684.9893
(0, 3)	148.213	188.1479	246.1573	335.3733	483.2215	755.3098	1343.100
(0, 4)	245.483	465.5756	407.2405	554.6590	799.0233	1248.800	2220.400
(0, 5)	367.174	650.5815	608.6237	828.7950	1193.800	1865.600	3317.000
(0, 6)	513.267	866.4487	850.3056	1157.800	1667.500	2605.800	4632.900

Table 3 Comparison of dimensionless linear frequency parameters of the perfect CCFGAP transverse vibration for various modes and inner to outer radius ratios ($\zeta = 0$, $k = 0$).

Results	Mode	b/a						
	(m, n)	0.1	0.2	0.3	0.4	0.5	0.6	0.7
Leissa [82]	(0, 1)	27.3000	–	45.2000	–	89.2000	–	248.0000
Vera et al. [83]		27.2800	–	45.3460	–	89.2500	–	248.4020
Han and Liew [84]		–	–	–	61.8710	–	–	–
Zhou et al. [85]		–	34.6090	–	61.8720	–	139.6100	–
Present study		**27.2805**	**34.6093**	**45.3462**	**61.8722**	**89.2508**	**139.6191**	**248.4021**
Leissa [82]	(1, 1)	28.4000	–	46.6000	–	90.2000	–	249.0000
Vera et al. [83]		28.9150	–	46.6430	–	90.2300	–	249.1640
Han and Liew [84]		–	–	–	–	–	–	–
Zhou et al. [85]		–	36.1030	–	62.9960	–	140.4800	–
Present study		**28.9158**	**36.1032**	**46.6435**	**62.9959**	**90.2303**	**140.4796**	**249.1639**
Leissa [82]	(2, 1)	36.7000	–	51.0000	–	93.3000	–	251.0000
Vera et al. [83]		36.6170	–	51.1380	–	93.3210	–	251.4800
Han and Liew [84]		–	–	–	–	–	–	–
Zhou et al. [85]		–	41.8200	–	66.6720	–	143.1300	–
Present study		**36.6173**	**41.8196**	**51.1388**	**66.6716**	**93.3212**	**143.1339**	**251.4806**
Leissa [82]	(3, 1)	51.2000	–	60.0000	–	99.0000	–	256.0000
Han and Liew [84]		–	–	–	–	–	–	–
Zhou et al. [85]		–	53.3880	–	73.6300	–	147.7900	–
Present study		**51.2188**	**53.3875**	**60.0335**	**73.6301**	**98.9280**	**147.7869**	**255.4438**

Table 4 First six dimensionless linear frequency parameters of the perfect CCFGAP in-plane axisymmetric vibration for various inner and outer radius ratios ($\zeta = 0$, $k = 0$).

Mode	b/a						
(m, n)	0.1	0.2	0.3	0.4	0.5	0.6	0.7
(0, 1)	15.5307	17.9412	22.1436	29.0640	40.8717	62.8849	110.712
(0, 2)	53.7362	64.8879	82.8865	111.465	159.380	247.974	439.711
(0, 3)	115.526	142.241	183.686	248.579	356.790	556.407	988.027
(0, 4)	201.316	250.304	324.716	440.500	633.146	988.203	1755.70
(0, 5)	311.286	389.154	506.016	687.247	988.454	1543.40	2742.60
(0, 6)	445.518	558.821	727.585	988.825	1422.70	2221.90	3948.90

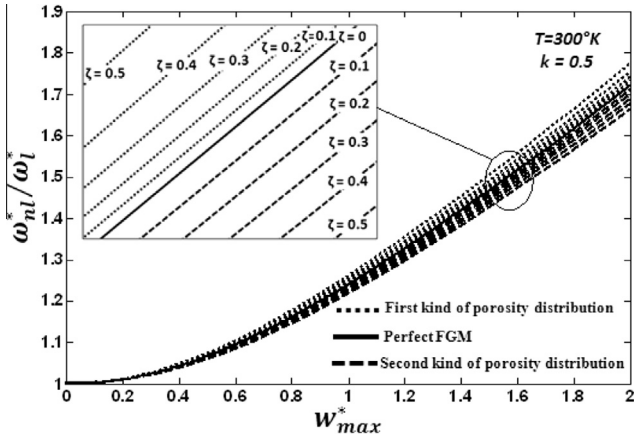

Figure 4 Effects of the porosity volume fraction on the non-linear frequencies associated with the CCFGAP fundamental non-linear axisymmetric mode shape.

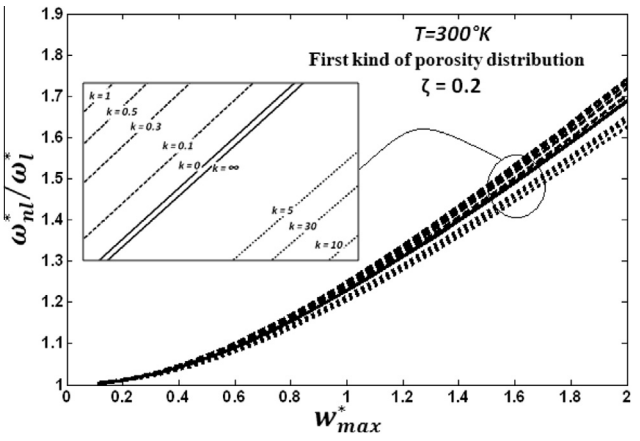

Figure 5 Effects of the gradient index on the non-linear frequencies associated with the imperfect CCFGAP fundamental non-linear axisymmetric mode shape.

Table 5 Non-linear dimensionless frequency ratios (ω^*_{nl}/ω^*_l) associated with the CCFGAP fundamental non-linear axisymmetric mode shape ($\alpha = 0.1$, $k = 0.5$).

w^*_{max}	First kind of porosity distribution $\zeta = 0.2$	Perfect FGM $\zeta = 0$	Second kind of porosity distribution $\zeta = 0.2$
0.02	1.0001	1.0001	1.0001
0.1	1.0029	1.0028	1.0027
0.2	1.0116	1.0114	1.0109
0.3	1.0259	1.0253	1.0243
0.4	1.0454	1.0444	1.0427
0.5	1.0696	1.0682	1.0656
0.6	1.0982	1.0962	1.0926
0.7	1.1305	1.1279	1.1232
0.8	1.1661	1.1629	1.1571
0.9	1.2045	1.2006	1.1936
1.0	1.2455	1.2409	1.2327
1.3	1.3794	1.3728	1.3608
1.5	1.4759	1.4679	1.4533
1.7	1.5763	1.5669	1.5497
1.9	1.6799	1.6690	1.6494
2.0	1.7325	1.7210	1.7000

$$2a_i k^w_{ir} + 3a_i a_j a_k b^w_{ijkr} + \frac{3}{2} a_i b_k C^{uw}_{irk} - 2\omega^2 a_i m^w_{ir} = 0, \quad r = 1, \ldots, po \tag{40a}$$

$$\frac{3}{4}\left(a_i a_j C^{uw}_{ijs} + 2b_i k^u_{is}\right) - 2\omega^2 b_i m^u_{is} = 0, \quad s = 1, \ldots, pi \tag{40b}$$

To simplify the analysis and the numerical treatment of the set of non-linear algebraic equations, a non-dimensional formulation has been considered by putting the spatial displacement functions as follows:

$$w_i(r) = h w^*_i(r^*), \quad u_i(r) = \lambda h u^*_i(r^*), \quad \lambda = \frac{h}{a}, \quad \alpha = \frac{b}{a} \tag{41}$$

To obtain non-dimensional parameters, the following relations can be put as such:

$$\frac{r}{r^*} = a, \quad \frac{z}{z^*} = h, \quad \left(m^u_{ij}, m^w_{ij}\right) = 2\pi I_0 h^2 a^2 \left(\lambda^2 m^{u*}_{ij}, m^{w*}_{ij}\right)$$
$$\frac{k^w_{ij}}{k^{w*}_{ij}} = \frac{k^u_{ij}}{k^{u*}_{ij}} = \frac{C^{uw}_{ijk}}{C^{uw*}_{ijk}} = \frac{b^w_{ijkl}}{b^{w*}_{ijkl}} = \frac{2\pi\overline{D_{11}}h^2}{a^2}, \quad \frac{\omega^2}{\omega^{*2}} = \frac{\overline{D_{11}}}{I_0 a^4} \tag{42}$$
$$\frac{K_L}{K^*_L} = \frac{2\overline{D_{11}}}{a^4}, \quad \frac{K_S}{K^*_S} = \frac{2\overline{D_{11}}}{a^2}, \quad \frac{K_{NL}}{K^*_{NL}} = \frac{4\overline{D_{11}}}{a^4 h^2}$$

Eqs. (40a) and (40b) can be written in a non-dimensional form as follows:

$$2a_i k^{w*}_{ir} + 3a_i a_j a_k b^{w*}_{ijkr} + \frac{3}{2} a_i b_k C^{uw*}_{irk} - 2\omega^{*2} a_i m^{w*}_{ir} = 0, \quad r = 1, \ldots, po \tag{43a}$$

$$\frac{3}{4}\left(a_i a_j C^{uw*}_{irs} + 2b_i k^{u*}_{is}\right) - 2\lambda^2 \omega^{*2} b_i m^{u*}_{is} = 0, \quad s = 1, \ldots, pi \tag{43b}$$

The non-dimensional terms $m^{w*}_{ij}, m^{u*}_{ij}, k^{w*}_{ij}, k^{u*}_{ij}, C^{uw*}_{ijk}$ and b^{w*}_{ijkl} are given by:

$$m^{w*}_{ij} = \int_\alpha^1 w^*_i w^*_j r^* dr^* \tag{44}$$

$$m^{u*}_{ij} = \int_\alpha^1 u^*_i u^*_j r^* dr^* \tag{45}$$

$$k^{w*}_{ij} = \int_\alpha^1 \left(\frac{d^2 w^*_i}{dr^{*2}}\frac{d^2 w^*_j}{dr^{*2}} + \frac{1}{r^{*2}}\frac{dw^*_i}{dr^*}\frac{dw^*_j}{dr^*}\right) r^* dr^* + K^*_L \int_\alpha^1 w^*_i w^*_j r^* dr^* + K^*_S \int_\alpha^1 \frac{dw^*_i}{dr^*}\frac{dw^*_j}{dr^*} r^* dr^* \tag{46}$$

$$k^{u*}_{ij} = \beta \int_\alpha^1 \left(\frac{du^*_i}{dr^*}\frac{du^*_j}{dr^*} + \frac{1}{r^{*2}} u^*_i u^*_j + \frac{v}{r^*}\frac{du^*_i}{dr^*} u^*_j + \frac{v}{r^*} u^*_i \frac{du^*_j}{dr^*}\right) r^* dr^* \tag{47}$$

$$C^{uw*}_{ijk} = \beta \int_\alpha^1 \left(\frac{dw^*_i}{dr^*}\frac{dw^*_j}{dr^*}\frac{du^*_k}{dr^*} + \frac{v}{r^*}\frac{dw^*_i}{dr^*}\frac{dw^*_j}{dr^*} u^*_k\right) r^* dr^* \tag{48}$$

$$b^{w*}_{ijkl} = \gamma \int_\alpha^1 \left(\frac{dw^*_i}{dr^*}\frac{dw^*_j}{dr^*}\frac{dw^*_k}{dr^*}\frac{dw^*_l}{dr^*}\right) r^* dr^* + K^*_{NL} \int_\alpha^1 w^*_i w^*_j w^*_k w^*_l r^* dr^* \tag{49}$$

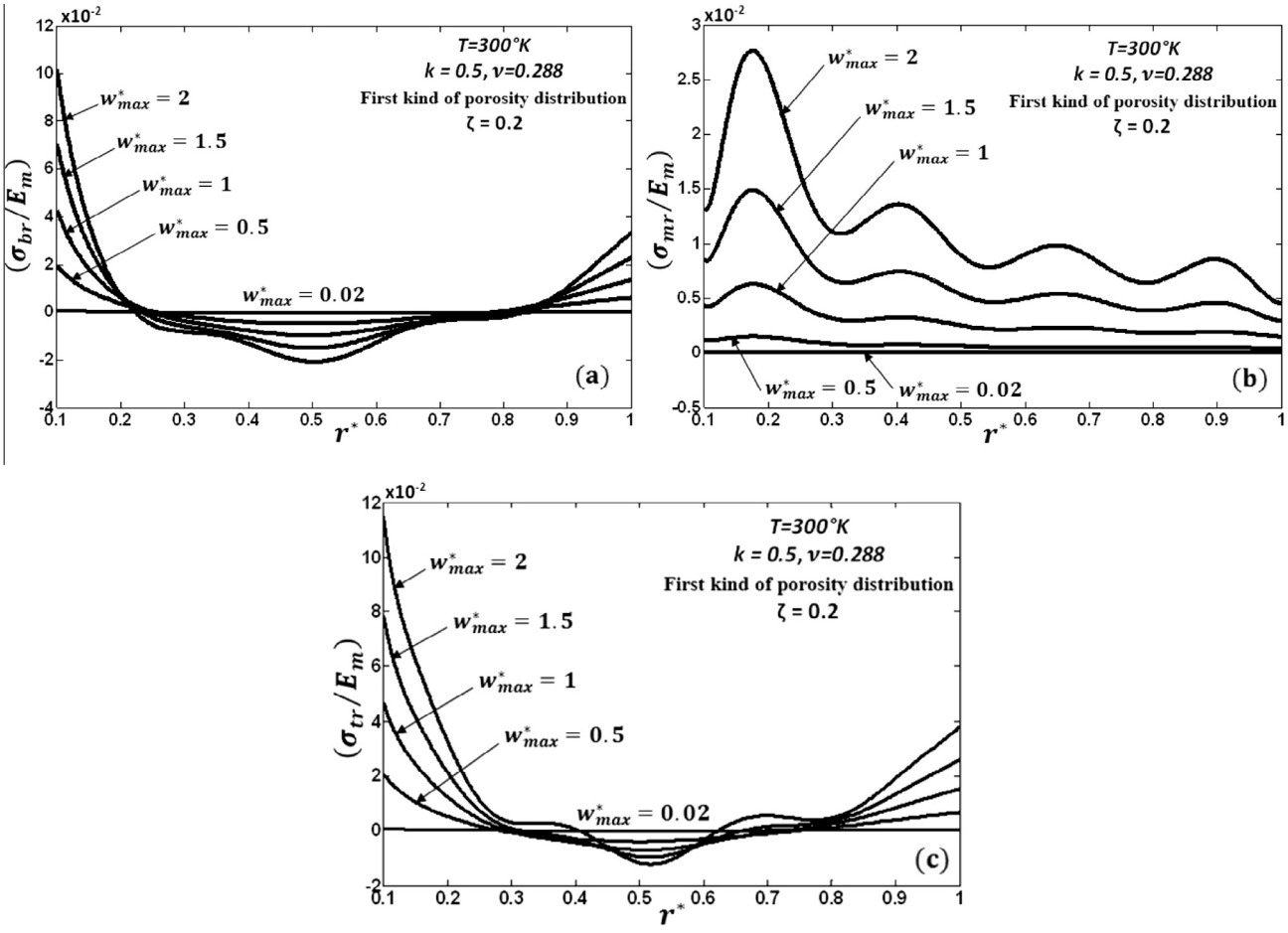

Figure 6 (a) Radial bending stress distribution, (b) radial membrane stress distribution, and (c) radial total stress distribution along the non-dimensional radius associated with the imperfect CCFGAP fundamental non-linear axisymmetric mode shape, at various dimensionless maximum vibration amplitudes.

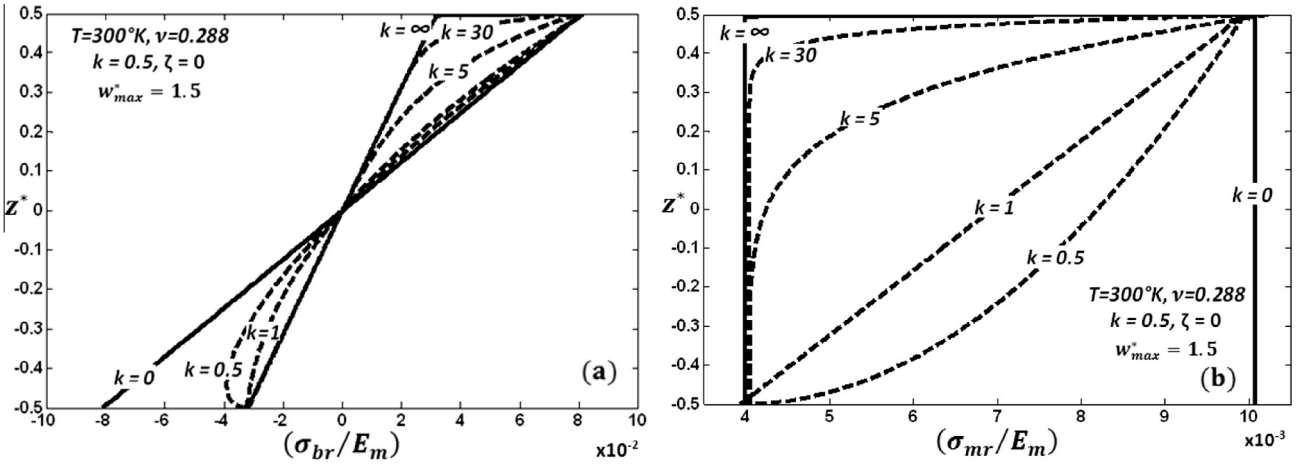

Figure 7 Effects of the gradient index on the distribution through the plate thickness of (a) the radial bending stress and (b) the radial membrane stress associated with the perfect CCFGAP fundamental non-linear axisymmetric mode shape at the inner edge of the plate.

with:

$$\beta = \frac{A_{11}h^2}{D_{11}}, \quad \gamma = \frac{A_{11}h^2}{4D_{11}} \tag{50}$$

In the case of thin plates, for which λ is very small, the in-plane inertia term, involving the term λ^2, can be neglected. This is an acceptable assumption in most engineering applications of thin

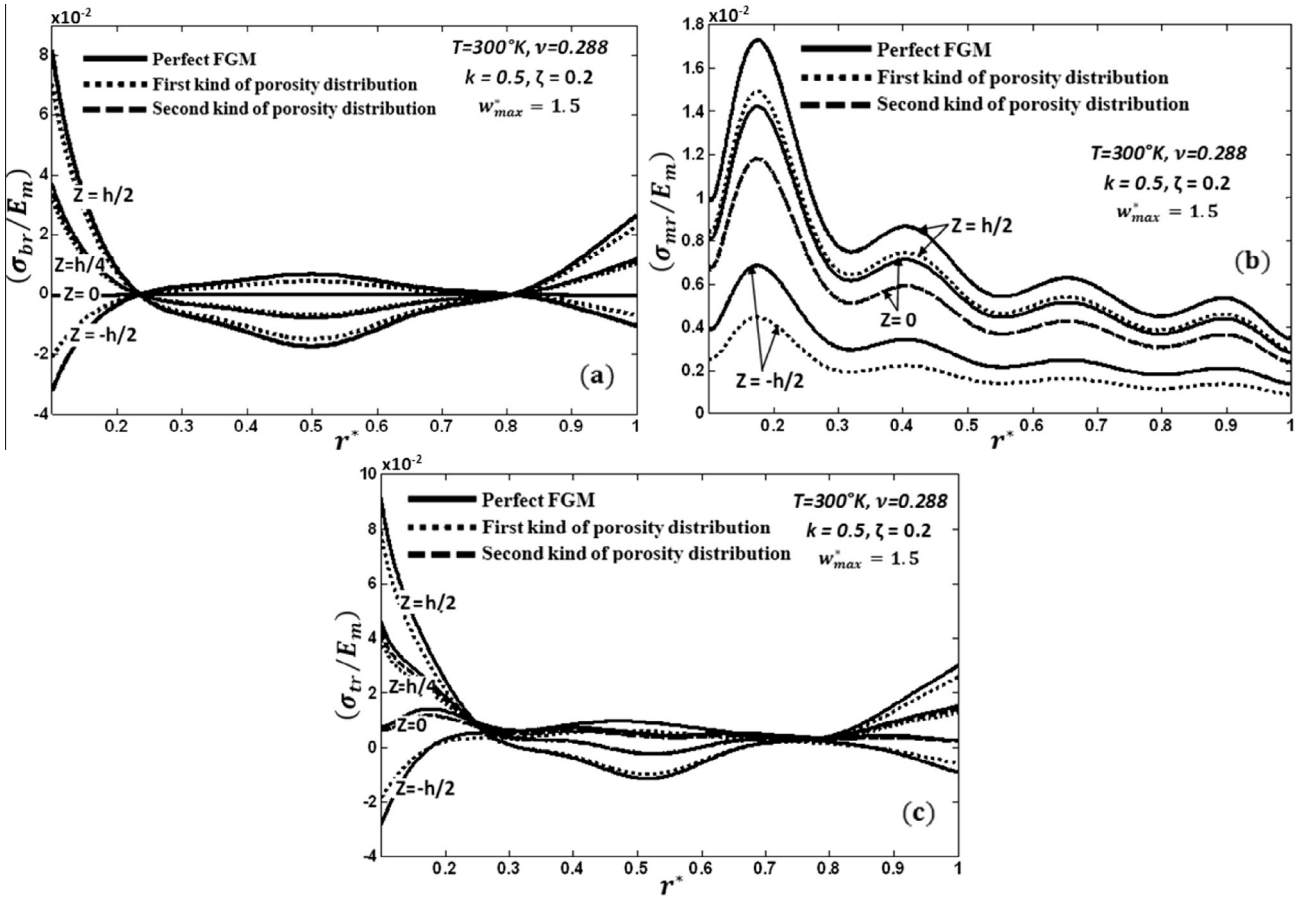

Figure 8 (a) Radial bending stress distribution, (b) radial membrane stress distribution, and (c) radial total stress distribution along the non-dimensional radius associated with the imperfect CCFGAP fundamental non-linear axisymmetric mode shape, at different levels of the plate cross section.

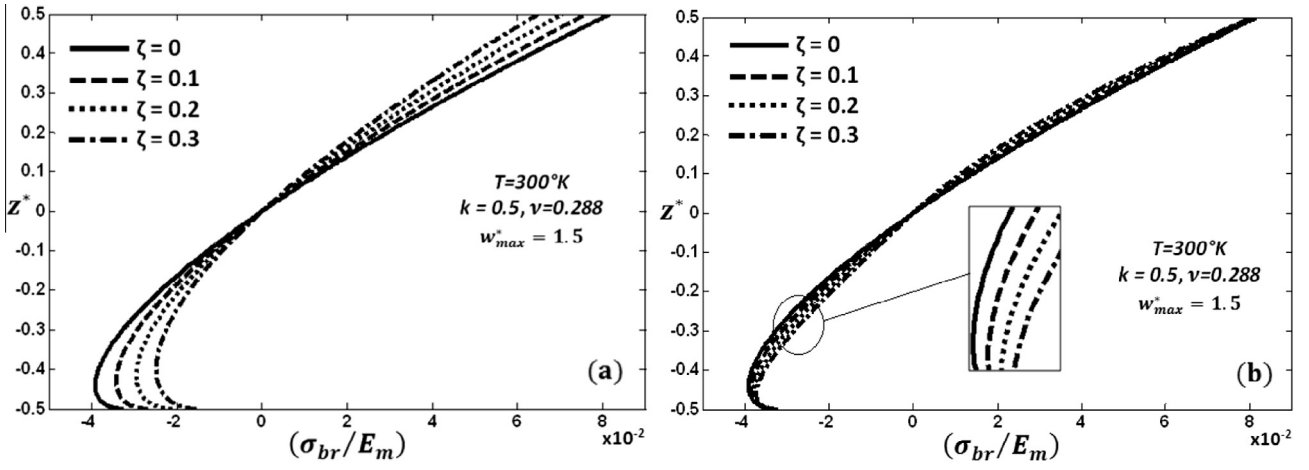

Figure 9 Effects of the porosity volume fraction on the distribution through the plate thickness of the radial bending stress associated with the perfect CCFGAP fundamental non-linear axisymmetric mode shape at the inner edge of plate: (a) first kind of porosity distribution and (b) second kind of porosity distribution.

plates [78]. Consequently, Eq. (43b) can be solved for the b_i's leading to:

$$b_i = a_j a_l d^*_{jli}, \quad i = 1, \ldots, pi \tag{51}$$

where

$$d^*_{ijk} = -\frac{1}{2} k^{u*-1}_{ij} C^{uw*}_{ijk} \tag{52}$$

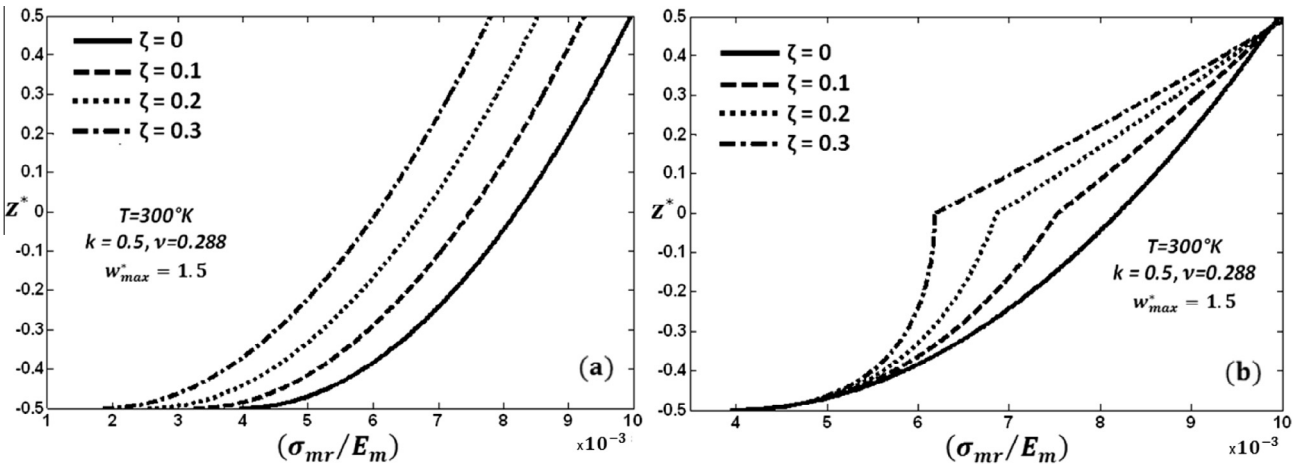

Figure 10 Effects of the porosity volume fraction on the distribution through the plate thickness of the radial membrane stress associated with the perfect CCFGAP fundamental non-linear axisymmetric mode shape at the inner edge of plate: (a) first kind of porosity distribution and (b) second kind of porosity distribution.

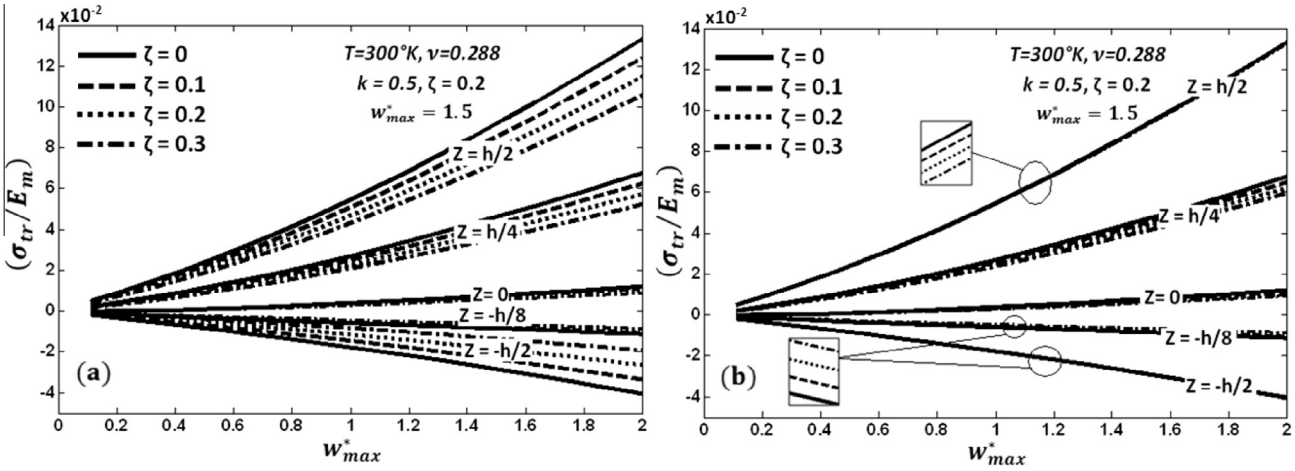

Figure 11 Effects of the porosity volume fraction on the radial total stress associated with the imperfect CCFGAP fundamental non-linear axisymmetric mode shape at the inner edge of the plate, for different levels of the plate cross section: (a) first kind of porosity distribution and (b) second kind of porosity distribution.

d^*_{ijk} is a third order tensor expressing the coupling between the in-plane and transverse vibrations and k^{u*-1}_{ij} is the inverse of the tensor k^{u*}_{ij}. Substituting Eq. (51) in Eq. (43a) leads to an uncoupled set of non-linear algebraic equations in terms of the a_i's coefficients only ($i = 1, \ldots, po$):

$$a_i k^{w*}_{ir} + \frac{3}{2} a_i a_j a_k b^*_{ijkr} - \omega^{*2} a_i m^{w*}_{ir} = 0, \quad r = 1, \ldots, po \tag{53}$$

where b^*_{ijkr} is a fourth order tensor given by:

$$b^*_{ijkl} = b^{w*}_{ijkl} + \frac{1}{2} C^{uw*}_{ijn} d^*_{kln} \tag{54}$$

The CCFGAP geometrically non-linear vibration problem is now described by Eq. (53) which is identical to that of an isotropic homogeneous annular plate having the equivalent parameters defined above. Eq. (53) can be written in matrix form as follows:

$$[K^{w*}]\{A\} + [Knl^*]\{A\} - \omega^{*2}[M^{w*}]\{A\} = \{0\} \tag{55}$$

where $[M^{w*}]$, $[Kl^{w*}]$ and $[Knl^*]$ are the non-dimensional mass matrix, the non-dimensional linear stiffness matrix and the dimensionless non-linear geometrical stiffness matrix respectively, and which have been computed numerically by a routine called PREP. Each term of the matrix $[Knl^*]$ is a quadratic function of the column matrix of coefficients $\{A\}^T = [a_1, a_2, \ldots\ldots, a_{po}]$, and is given by $Knl^*_{ij} = (3/2)a_k a_l b^*_{ijkl}$. It may be worth noticing that, when the non-linear term is neglected in Eq. (70), it reduces to the eigenvalue problem:

$$[Kl^{w*}]\{A\} - \omega^{*2}[M^{w*}]\{A\} = \{0\} \tag{56}$$

which is the Rayleigh–Ritz formulation of the linear vibration problem.

In order to obtain the numerical solution for the non-linear problem in the neighborhood of a given mode, the contribution of this mode is chosen and those of other modes are calculated numerically using the Harwell library routine NS01A, to obtain the numerical results presented for the r_0th

non-linear mode shape of CCFGAP. For the first mode, the procedure consisted of fixing a_1 and calculating the higher mode contributions from the system:

$$a_i k_{ir}^{w*} + \frac{3}{2} a_i a_j a_k b_{ijkr}^{*} - \omega^{*2} a_i m_{ir}^{w*} = 0, r > 1 \tag{57}$$

in which ω^{*2} is obtained either, from the principle of conservation of energy ($V_{max} = T_{max}$) applied by Benamar and co-authors [53,59,64,66] to many non-linear structural dynamic cases, where V_{max} is the maximum value of the total strain energy obtained from Eq. (30) for $t = 2\pi/\omega$, at which $T = 0$, and T_{max} is the maximum value of the kinetic energy obtained from Eq. (31), for $t = \pi/(2\omega)$, at which $T = 0$, or from another formula for the "non-linear Rayleigh quotient", that is based on an alternative mathematical procedure similar to that used in the linear case. It consists on pre-multiplying Eq. (57) by $\{A\}^T$ and then deducing the expression for the dimensionless non-linear frequency ω^* as follows:

$$\omega^{*2} = \left(a_i a_j k_{il}^{w*} + (3/2) a_i a_j a_k a_l b_{ijkl}^{*} \right) / a_i a_j m_{ij}^{w*} \tag{58}$$

2.3.6. Iterative numerical procedure

The Harwell library routine NS01A is based on a hybrid iterative method combining the steepest descent and Newton's methods. This method does not require a very good initial estimate of the solution [81]. A step procedure, similar to that described in Refs. [71–73] for fully clamped beams and rectangular isotropic and laminated plates is adopted here to ensure a rapid convergence while varying the amplitude, which allowed solutions to be obtained with a quite reasonable number of iterations (an average of 28 for ($po = 6$) non-linear algebraic equations used in this work). For the first non-linear axisymmetric mode shape, the first calculation was made in the neighborhood of the linear solution by attributing a small numerical value (a) to the coefficient a_1 of the basic function w_1^*. The resulting solution was then used as an initial estimate for the following step corresponding to ($a + \Delta a$). Thus, by choosing in each case the convenient value of the step (Δa), the first non-linear axisymmetric mode shape has been calculated at various maximum vibration amplitudes extending up to a given value. The limit of error residuals is imposed to be lower than 10^{-16} in all cases. For the first non-linear axisymmetric mode and for a given amplitude of vibration w_{max}^*, the numerical iterative procedure accurately determines the non-dimensional non-linear frequency parameter ω^* and the corresponding normalized eigenvector $\{A\}^T = [a_1, \ldots, a_6]$ which in turn gives the first non-linear axisymmetric mode shape: $w^*(r^*) = a_i w_i^*(r^*), i = 1, \ldots, 6$. The corresponding in-plane shape function, i.e., $u^*(r^*) = b_i u_i^*(r^*), i = 1, \ldots, 6$, is determined

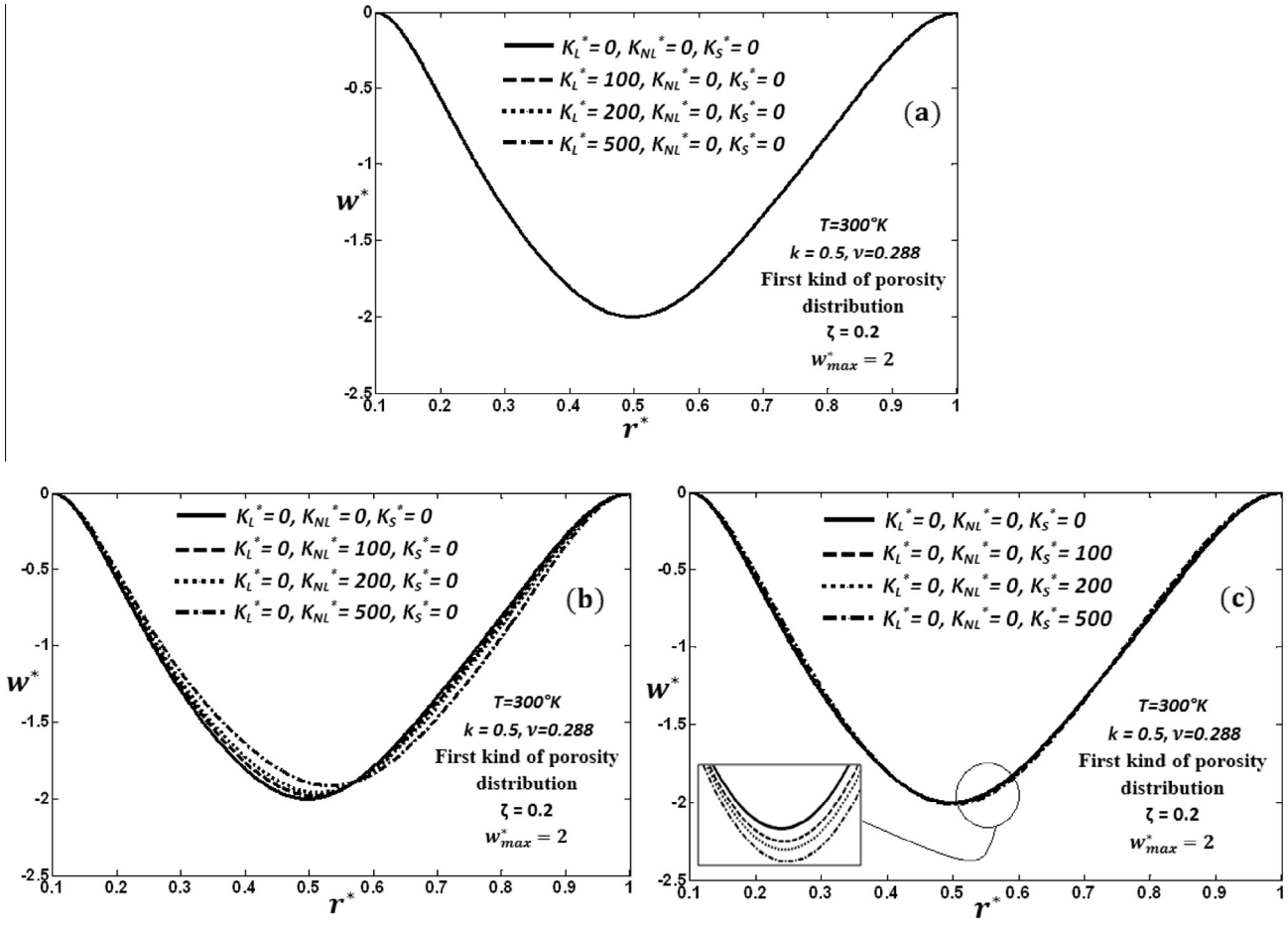

Figure 12 Effects of the elastic foundation parameters on the fundamental non-linear axisymmetric mode shape of the imperfect CCFGAP: (a) Winkler foundation parameter, (b) non-linear foundation parameter, and (c) shear layer foundation parameter.

by computing the in-plane contribution coefficients b_i from Eq. (51). In addition, the associated non-linear bending and membrane stresses can be determined quite easily.

2.4. Bending, membrane and total stress expressions

By using the classical thin plate assumption of plane stress and Hooke's law, the radial and circumferential bending stresses in the annular plate are given below:

$$\sigma_{br} = -\frac{zE(z)}{(1-v^2)}\left[\frac{d^2w}{dr^2}+\frac{v}{r}\frac{dw}{dr}\right] \tag{59}$$

$$\sigma_{b\theta} = -\frac{zE(z)}{(1-v^2)}\left[\frac{1}{r}\frac{dw}{dr}+v\frac{d^2w}{dr^2}\right] \tag{60}$$

And the radial and circumferential membrane stresses are given by:

$$\sigma_{mr} = \frac{E(z)}{(1-v^2)}\left[\frac{du}{dr}+\frac{1}{2}\left(\frac{dw}{dr}\right)^2+v\frac{u}{r}\right] \tag{61}$$

$$\sigma_{m\theta} = \frac{E(z)}{(1-v^2)}\left[\frac{u}{r}+v\left(\frac{du}{dr}+\frac{1}{2}\left(\frac{dw}{dr}\right)^2\right)\right] \tag{62}$$

The radial total stress is defined as follows:

$$\sigma_{tr} = \sigma_{mr} + \sigma_{br} \tag{63}$$

In terms of the non-dimensional parameters defined in the previous section, the radial and circumferential bending stresses σ_{br} and $\sigma_{b\theta}$ can be defined as follows:

$$\sigma_{br} = -\frac{z^*E(z^*)}{(1-v^2)}\frac{h^2}{a^2}\left[\frac{d^2w^*}{dr^{*2}}+\frac{v}{r^*}\frac{dw^*}{dr^*}\right] \tag{64}$$

$$\sigma_{b\theta} = -\frac{z^*E(z^*)}{(1-v^2)}\frac{h^2}{a^2}\left[\frac{1}{r^*}\frac{dw^*}{dr^*}+v\frac{d^2w^*}{dr^{*2}}\right] \tag{65}$$

$$\sigma_{mr} = \frac{E(z^*)}{(1-v^2)}\frac{h^2}{a^2}\left[\frac{du^*}{dr^*}+\frac{1}{2}\left(\frac{dw^*}{dr^*}\right)^2+v\frac{u^*}{r^*}\right] \tag{66}$$

$$\sigma_{m\theta} = \frac{E(z^*)}{(1-v^2)}\frac{h^2}{a^2}\left[\frac{u^*}{r^*}+v\left(\frac{du^*}{dr^*}+\frac{1}{2}\left(\frac{dw^*}{dr^*}\right)^2\right)\right] \tag{67}$$

2.5. Basic functions choice

The problem of transverse vibrations of the thin annular plates requires the solution of transcendental equations involving ordinary and modified Bessel functions of the first and second kinds of order as explained in [82]. The axisymmetric CCFGAP transverse basic functions $w_i^*(r^*)$ are given below:

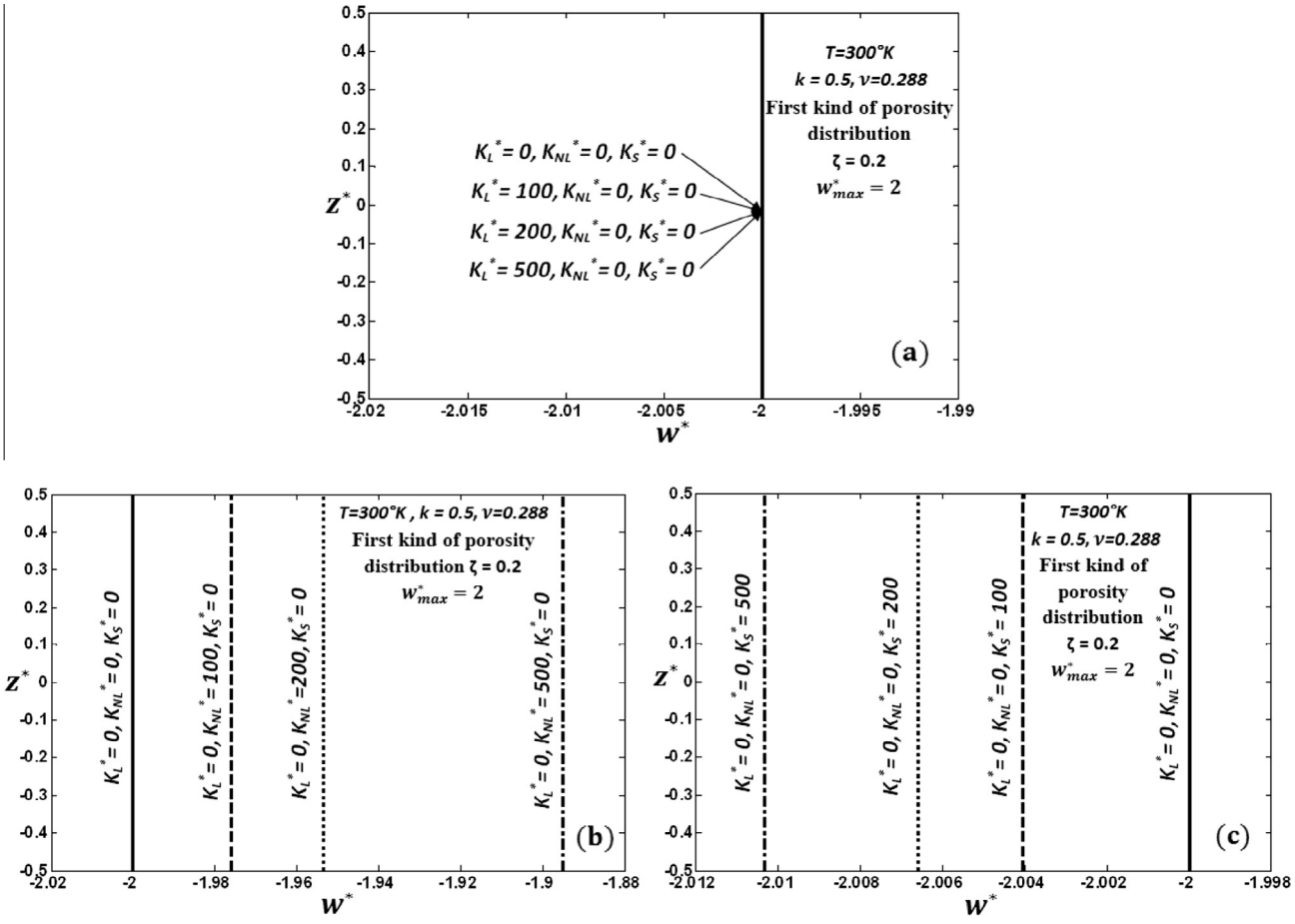

Figure 13 Effects of the elastic foundation parameters on the distribution through the plate thickness of the transverse displacement of the imperfect CCFGAP: (a) Winkler foundation parameter, (b) non-linear foundation parameter, and (c) shear layer foundation.

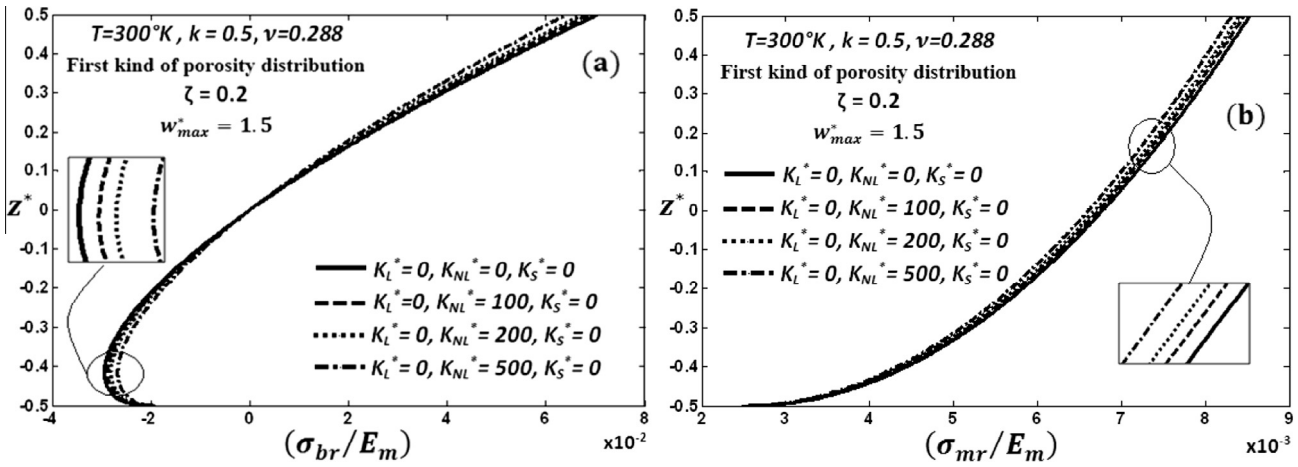

Figure 14 Effects of the non-linear foundation parameter on the distribution through the plate thickness of (a) the radial bending stress and (b) the radial membrane stress, at the inner edge of the imperfect CCFGAP.

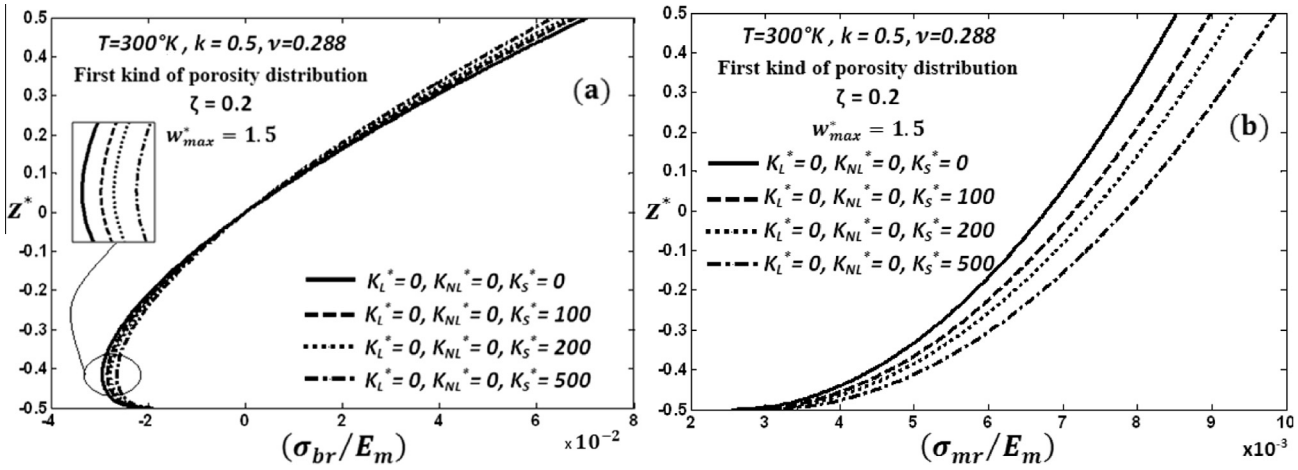

Figure 15 Effects of the shear layer foundation parameter on the distribution through the plate thickness of (a) the radial bending stress and (b) the radial membrane stress, at the inner edge of the imperfect CCFGAP.

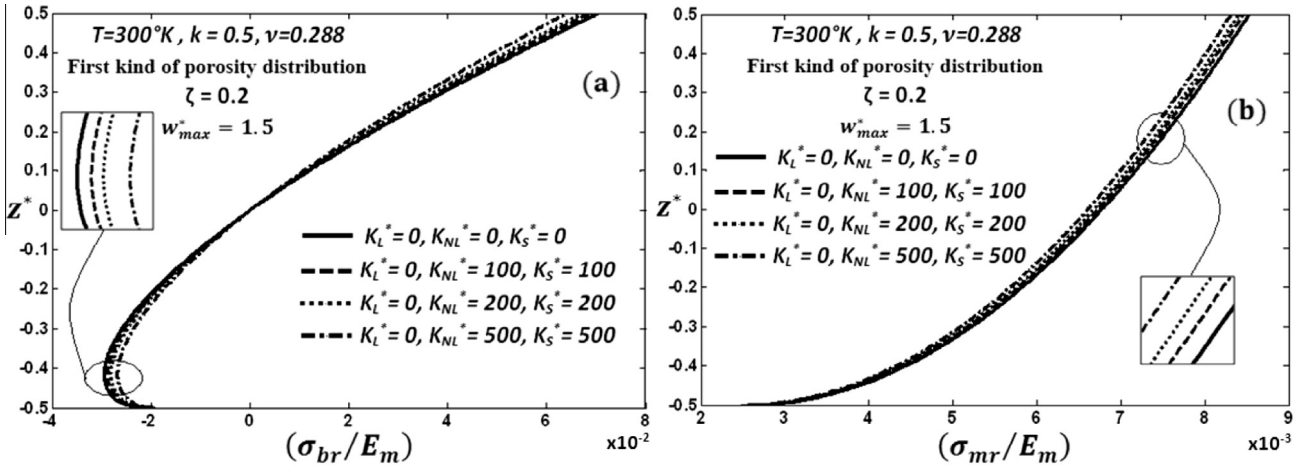

Figure 16 Effects of the combination of non-linear foundation parameter with shear layer foundation parameter on the distribution through the plate thickness of (a) the radial bending stress and (b) the radial membrane stress, at the inner edge of the imperfect CCFGAP.

$$w_i^*(r^*) = A_i[J_0(\eta_i r^*) + B_i Y_0(\eta_i r^*) + C_i I_0(\eta_i r^*) + D_i K_0(\eta_i r^*)] \tag{68}$$

where A_i is chosen as follows:

$$\int_\alpha^1 w_i^{*2} r^* dr^* = 1 \tag{69}$$

and the eigenvalues η_i are obtained from the fourth-order determinant of the homogeneous system which is obtained by applying the boundary conditions at each edge of the annular plate. The constants B_i, C_i and D_i are obtained by back-substitution of the eigenvalues in the usual manner. η_i is related to the ith dimensionless linear frequency parameter of the annular plate transverse axisymmetric vibration by:

$$\eta_i^2 = (\omega_{lw}^*)_i \tag{70}$$

Numerical results for the first six linear frequency parameters of the annular plate with clamped edges transverse axisymmetric vibration for various inner to outer radius ratios are summarized in Table 2. The comparisons of the results obtained here and those found in [82–85] are illustrated in Table 3, for various linear modes (m, n) and inner to outer radius ratios. It is observed that the present results are almost identical to those reported by these references.

The chosen in-plane basic functions $u_i^*(r^*)$ for the axisymmetric vibration of the annular plate with clamped outer and inner edge are given by [86].

$$u_i^*(r^*) = -\xi_i \left[J_1(\xi_i r^*) - \frac{J_1(\xi_i)}{Y_1(\xi_i)} Y_1(\xi_i r^*) \right] \tag{71}$$

where ξ_i is the ith real positive root of the transcendental equation:

$$J_1(\xi_i) Y_1(\alpha\xi_i) - J_1(\alpha\xi_i) Y_1(\xi_i) = 0 \tag{72}$$

ξ_i is related to the ith dimensionless linear frequency parameter of the annular plate in-plane axisymmetric vibration by:

$$\xi_i^2 = (\omega_{lu}^*)_i \tag{73}$$

Numerical results for the first six linear frequency parameters of the annular plate with clamped edges in-plane axisymmetric vibration for various inner to outer radius ratios are summarized in Table 4.

3. Numerical results and discussion

The effect of the porosity on the fundamental non-linear frequencies of CCFGAP is plotted in Fig. 4. As shown in this figure, the first kind of porosity distribution through the plate

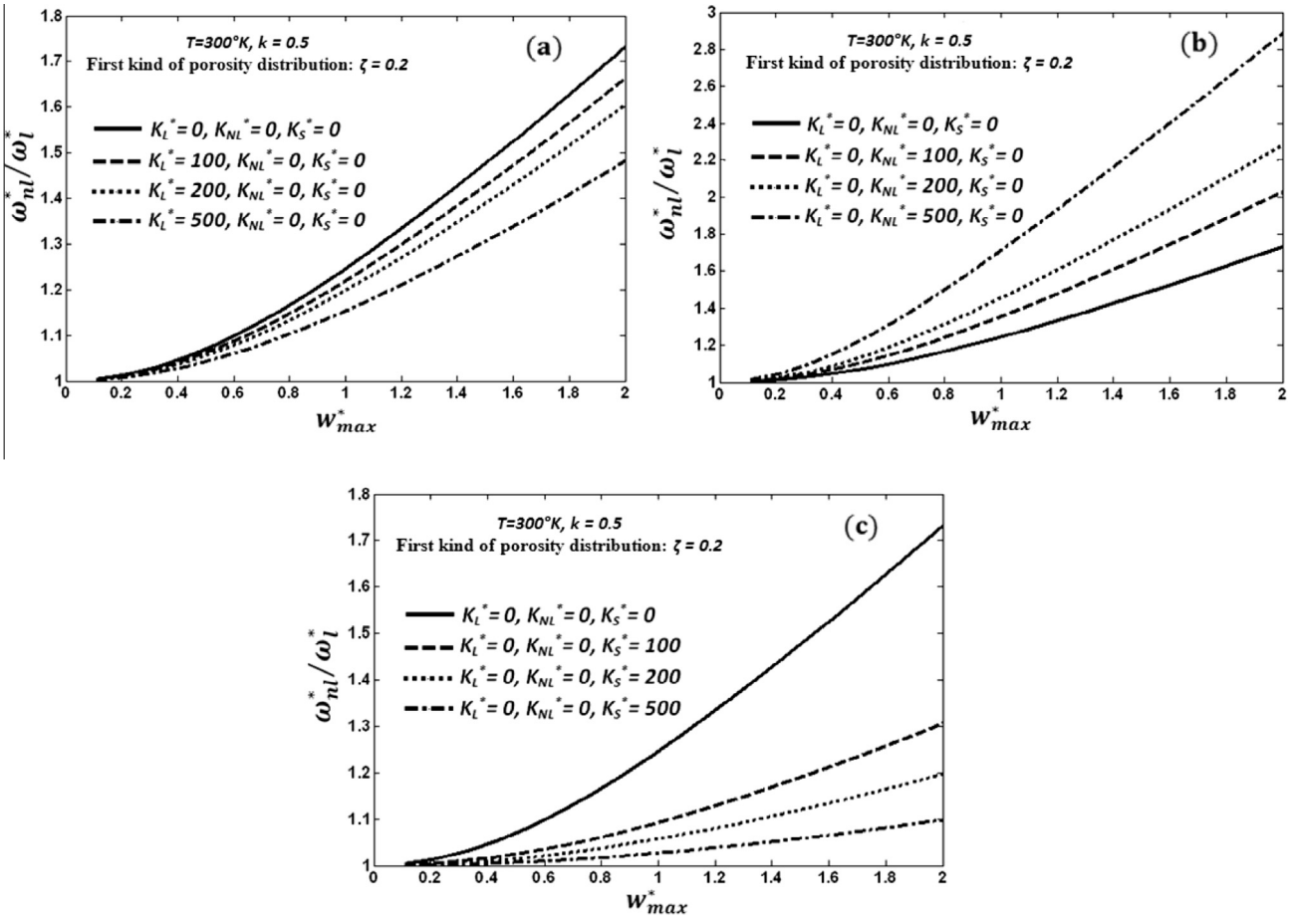

Figure 17 Effects of the elastic foundation parameters on the non-linear frequencies of the imperfect CCFGAP fundamental non-linear axisymmetric mode shape: (a) Winkler foundation parameter, (b) non-linear foundation parameter, and (c) shear layer foundation parameter.

thickness tends to increase the non-linear frequencies of the imperfect plate compared to the case of the perfect plate, when the porosity volume fraction ζ increases, while the second kind of porosity distribution tends to decrease them. A comparison between the dimensionless frequency ratios associated with the fundamental non-linear axisymmetric mode shape of the perfect and imperfect plate with the first and second kind of porosity distribution is illustrated in Table 5.

The effect of the gradient index on the non-linear frequencies of the imperfect CCFGAP is plotted in Fig. 5. For small vibration amplitudes, the variation in the gradient index has no significant effect on the frequencies associated with the fundamental non-linear axisymmetric mode shape, but at high vibration amplitudes, the non-linear frequencies increase for some values of the gradient index and decrease for other values.

The curves of Figs. 6 and 11 show the non-linear amplitude dependence of the stresses associated with the CCFGAP fundamental non-linear axisymmetric mode shape. Examination of Fig. 6(a)–(c), shows an increase in the stresses with increasing the amplitude of vibration with a higher and rapid increase in the radial bending and total stresses closer to the clamped edges, especially for the inner edge of the CCFGAP. The radial bending (σ_{br}) and membrane (σ_{mr}) stress distributions through the thickness at the inner edge of plate, for different values of gradient index (k), are plotted in Fig. 7(a) and (b) respectively. It is obvious that when the gradient index increases the variation of Young's modulus becomes increasingly abrupt through the thickness. Consequently, the stresses vary accordingly. It is observed that, for the completely ceramic-rich or metal-rich plates, corresponding respectively to $k = 0$ and $k = \infty$, the stress variation through the plate thickness is linear, while for the CCFGAP, the behavior is non-linear and is governed by the variation of the properties in the thickness direction.

An analysis of the effects of porosity on the stresses in the CCFGAP, particularly the effects of the kind of porosity distribution through the annular plate thickness, leads to the following remarks:

- It can be seen from Fig. 8(a)–(c) that the radial bending stress at the plate mid-plane ($z^* = 0$) is negligible. However, it may be noticed that the stresses are greater at the rich-ceramic surface ($z^* = +0.5$), compared to those at the rich-metal surface ($z^* = -0.5$). The stresses at the inner edge of the plate, associated with the second kind of porosity distribution, exhibits less change compared to the case of the first kind of porosity distribution.
- It can be seen from Figs. 9(a) and (b), and 10(a) and (b) that the stresses decrease with increasing porosity volume fraction (ζ) for the two kinds of porosity distribution considered.

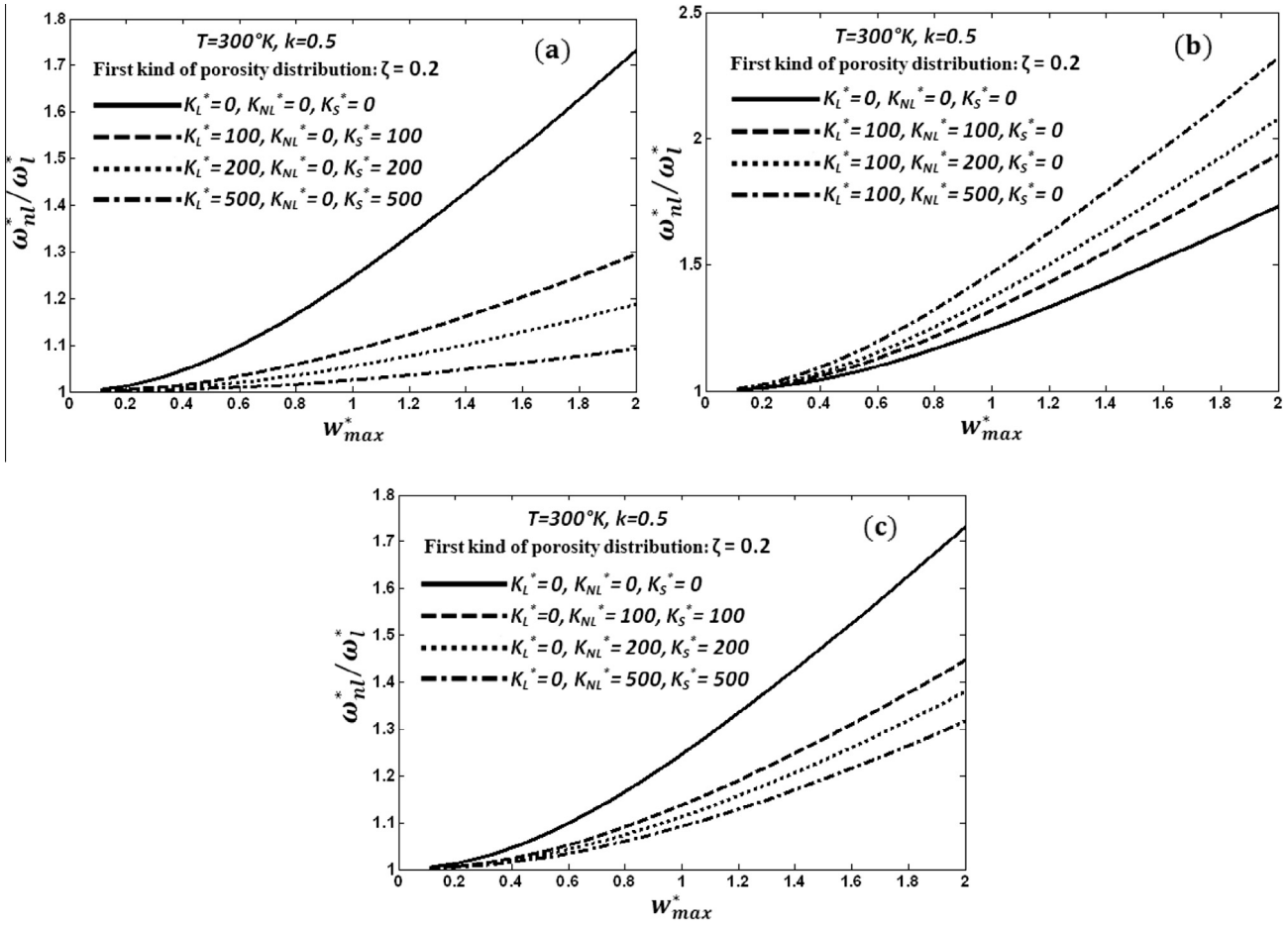

Figure 18 Effects of various elastic foundations on non-linear frequencies associated with the imperfect CCFGAP fundamental non-linear axisymmetric mode shape.

Table 6 Effect of the three elastic foundation parameters on the non-linear dimensionless frequency ratios $(\omega^*_{nl}/\omega^*_l)$ associated with the CCFGAP first two non-linear axisymmetric mode shapes, at various non-dimensional maximum amplitude of vibration ($\alpha = 0.1$, $\zeta = 0.2$, $k = 0.5$).

w^*_{max}	Mode	Elastic foundation type: K^*_L–K^*_{NL}–K^*_S						
	(m, n)	*0–0–0*	*100–0–0*	*500–0–0*	*0–100–0*	*0–500–0*	*0–0–100*	*0–0–500*
0.02	(0, 1)	1.00011	1.00010	1.00007	1.00017	1.00040	1.00004	1.00001
0.5		1.06969	1.06167	1.04224	1.10281	1.22461	1.02470	1.00693
1		1.24550	1.21900	1.15314	1.35506	1.71206	1.09227	1.02699
1.5		1.47593	1.42786	1.30569	1.67731	2.28343	1.18964	1.05813
2		1.73259	1.66275	1.48236	2.03024	2.88451	1.30633	1.09800
0.02	(0, 2)	1.00021	1.00020	1.00019	1.00021	1.00024	1.00010	1.00003
0.5		1.11928	1.11732	1.11010	1.12302	1.13953	1.06267	1.02191
1		1.37917	1.37350	1.35158	1.39245	1.44658	1.21026	1.07879
1.5		1.71130	1.70152	1.66509	1.73430	1.82061	1.41260	1.16314
2		2.07037	2.05911	2.00513	2.10439	2.26927	1.63985	1.26317

– As shown in Fig. 11(a) and (b), the effect of the porosity for the first kind is higher at both the rich-ceramic and rich-metal surfaces. It decreases if one moves toward the annular plate mid-plane, where the stresses vanish. For the second kind of porosity distribution, this effect is higher in the middle zones of the plate cross section and decreases to zero when one moves toward the bottom and the top of the plate cross section.

In order to analyze the effects of elastic foundation parameters on the displacements, the CCFGAP fundamental non-linear axisymmetric mode shape is plotted in Fig. 12(a)–(c) for the first kind of porosity distribution. The corresponding transverse displacement distributions through the plate thickness are plotted in Fig. 13(a)–(c). Results show that the non-linear and shear layer foundation parameters (K_{NL}) and (K_S) are more effective in reducing deflection than the Winkler foundation parameter (K_L). Increase in shear layer (K_S) and non-linear (K_{NL}) foundation parameters causes decrease in the plate deformation. The decrease in the displacement indicates that the increase in the foundation stiffness will certainly enhance the plate rigidity.

The radial and membrane stress distributions through the plate thickness at the inner edge are plotted in Figs. 14–16 for various elastic foundations. All curves show that, the radial membrane stress (σ_{mr}) is negligible compared to the radial bending stress (σ_{br}); therefore, it does not have any influence on the radial total stress (σ_{tr}). Fig. 14(a) and (b) shows that the increase in non-linear foundation parameter (K_{NL}) causes decrease in the radial bending (σ_{br}) and radial membrane (σ_{mr}) stresses, therefore, a decrease in the total radial stress (σ_{tr}). As can also be seen from Fig. 15, an increase in shear layer foundation parameter (K_S) causes, (a) a decrease in radial bending stress (σ_{br}), and (b) an increase in radial membrane stress (σ_{mr}). The rate of decrease or of an increase in stresses is higher at rich-ceramic surface than at the rich-metal surface of the plate. It can be observed from Fig. 16(a) and (b), that the radial bending (σ_{br}) and radial membrane (σ_{mr}) stresses decrease with increasing (K_{NL}, K_S). This appears logic since (σ_{mr}) is negligible compared to (σ_{br}).

In order to analyze the effect of the elastic foundation parameters on the non-linear frequencies of the CCFGAP, the frequency ratio variation, versus the maximum non-dimensional amplitude of vibration, and for various foundation parameters, is depicted in Figs. 17 and 18 for the fundamental non-linear axisymmetric mode shape, and is illustrated in Table 6 for both the first two non-linear axisymmetric mode shapes. All curves and Table 6 show the amplitude dependence of the non-linear frequencies as it has been shown in previous studies [53–69] for beams, shells and plate-like structures. As it can be seen from these figures and this table, the non-linear frequencies decrease with increasing (K_L, K_S) and increase with increasing (K_{NL}). The fundamental non-linear axisymmetric mode shape exhibits more decrease and increase in the frequencies than it does the second non-linear axisymmetric mode shape, and the rate of decrease and of increase increases with increasing the vibration amplitude. It is observed in Fig. 18 (b) that the increase of (K_L, K_{NL}) leads to an increase in the non-linear frequencies with the vibration amplitudes. However, the increase of (K_L, K_S) or (K_{NL}, K_S) leads to a decrease in the non-linear frequencies as shown in Fig. 18(a) and (c).

4. Conclusion

The geometrically non-linear free vibrations analysis of imperfect CCFGAP, resting on elastic foundations, with two types of porosity distribution through the plate thickness, have been presented using a semi analytical method based on Hamilton's principle and spectral analysis. A homogenization procedure, which has been proposed, reduces the examined problem to that of an equivalent isotropic homogeneous annular plate. The influence of the porosity volume fraction and its distribution through the plate thickness, the distribution of the material properties through the plate thickness and the elastic foundation parameters on non-linear vibration responses of the CCFGAP have been carefully examined and discussed. Concerning the effect of the geometrical non-linearity on the frequencies, the obtained curves show a non-linearity of the hardening type (i.e., the frequency increases with increasing the vibration amplitude). It is also shown that the geometrical non-linearity induces a deformation of the fundamental axisymmetric mode shape which induces a significant increase in the resulting stresses at the inner and outer plate edges. In view of the numerical results obtained, some concluding remarks may be formulated as follows:

- For small vibration amplitudes, porosity volume fraction (ζ) and the gradient index (k) have no significant effect on the frequencies and stresses associated with the CCFGAP fundamental non-linear axisymmetric mode shape, but it may have a considerable effect at high vibration amplitudes.
- The increase in the porosity volume fraction (ζ) causes an increase in the non-linear frequencies for the case of the first kind of porosity distribution through the plate thickness, and a decrease in the frequencies for the second kind of porosity distribution case.
- The increase in the porosity volume fraction (ζ) causes a decrease of Young's modulus of the plate for the two kinds of porosity distribution considered, and therefore leads to a decrease in the stresses in the plate.
- The variation of Young's modulus becomes increasingly abrupt through the plate thickness for higher values of the gradient index (k), and it consequently leads to an increase in the stresses in an abrupt manner.
- The analysis of the influence of the foundation parameters on the geometrically nonlinear free vibration response of CCGAP reveals that, for small vibration amplitudes, the foundation parameters have no significant effect except at high vibration amplitudes:
  - The CCFGAP deflections decrease with increasing the foundation parameters.
  - The effect of the shear layer and non-linear foundation parameters (K_S, K_{NL}) on the deformations reduction of CCFGAP is greater, compared with the case of the Winkler foundation parameter (K_L).
  - The Winkler foundation parameter (K_L) has no significant effect on the stresses associated with the fundamental non-linear axisymmetric mode shape.
  - The shear layer and non-linear foundation parameters (K_S, K_{NL}) reduce the radial total stress associated with the CCFGAP fundamental non-linear axisymmetric mode shape. (K_S) is more effective than (K_{NL}) in reducing the stresses in the plate.
  - The shear layer and Winkler foundation parameters (K_S, K_L) are more effective than non-linear foundation parameter (K_{NL}) on frequencies associated with the first two non-linear axisymmetric mode shapes.
  - The increase in the shear layer and Winkler foundation parameters (K_S, K_L) causes a decrease in frequencies associated with the first two non-linear axisymmetric mode shapes.
  - The increase in the non-linear foundation parameter (K_{NL}) causes an increase in frequencies associated with the first two non-linear axisymmetric mode shapes.
  - The effect of the foundation parameters on the non-linear frequencies associated with the first non-linear axisymmetric mode shape is more accentuated than that associated with the second non-linear axisymmetric mode shape, and this effect increases with increasing the vibration amplitude.

The gradient index, porosity volume fraction, type of porosity distribution through the plate thickness and elastic foundation parameters have a significant influence on the geometrically non-linear free vibration response of the CCFGAP at large amplitudes. Further investigations are needed to examine the effects of the porosity, the boundary conditions, and the elastic foundation parameters on the thermo-mechanical behavior of FGAP at large vibration amplitudes.

References

[1] Miyamoto Y, Kaysser WA, Rabin BH, Kawasaki A, Ford RG. Functionally graded materials design, processing and applications. Kluwer Academic Publishers; 1999.

[2] Dong YS, Lin PH, Wang HX. Electroplating preparation of Ni–Al_2O_3 graded composite coatings using a rotating cathode. Surf Coat Technol 2006;200(11):3633–6.

[3] Xiong HP, Kawasaki A, Kang YS, et al. Experimental study on heat insulation performance of functionally graded metal/ceramic coatings and their fracture behavior at high surface temperatures. Surf Coat Technol 2005;194(2–3):203–14.

[4] Butcher RJ, Rousseau CE, Tippur HV. A functionally graded particulate composite: preparation, measurements and failure analysis. Acta Mater 1998;47(1):259–68.

[5] Yaghoobi H, Feridoon A. Influence of neutral surface position on deflection of functionally graded beam under uniformly distributed load. World Appl Sci J 2010;10(3):337–41.

[6] Birman V, Byrd LW. Modeling and analysis of functionally graded materials and structures. Appl Mech Rev 2007; 60:195–216.

[7] Kudesia R, Niedzialek SE, Stangle GC, McCauley JW, Richard M, Kaieda Y. Design and fabrication of TiC/NiAI functionally gradient materials for joining applications. In: Wachtman John B. editor. 16th Annual conference on composites and advanced ceramic materials, vol. 13(7–8). Wiley; 2010. p. 383–374.

[8] Khor KA, Gu YW. Effects of residual stress on the performance of plasma sprayed functionally graded ZrO_2/ NiCoCrAlY coatings. Mater Sci Eng A 2000;277(1–2):64–76.

[9] Seifried S, Wintere MR, Hahn H. Nanocrystalline graded films through chemical vapor synthesis. Scripta Mater 2001;44(8–9):2165–8.

[10] Watanabe, Eryu YH, Matsuura K. Evaluation of three dimensional orientation of Al_3Ti platelet in Al-based functionally graded materials fabricated by a centrifugal casting technique. Acta Mater 2001;49(5):775–83.

[11] Song C, Xu Z, Li J. Structure of in situ Al/Si functionally graded materials by electromagnetic separation method. Mater Des 2007;28(3):1012–5.

[12] Peng X, Yan M, Shi W. A new approach for the preparation of functionally graded materials via slip casting in a graded magnetic field. Scripta Mater 2007;56(10):907–9.

[13] Zhu J, Lai Z, Yin Z, Jeon J, Lee S. Fabrication of ZrO_2NiCr functionally graded material by powder metallurgy. Mater Chem Phys 2001;68:130–5.

[14] Ying J, Lü CF, Chen WQ. Two-dimensional elasticity solutions for functionally graded beams on elastic foundations. Compos Struct 2008;84:209–19.

[15] Pradhan SC, Murmu T. Thermo-mechanical vibration of FGM sandwich beam under variable elastic foundations using differential quadrature method. J Sound Vib 2009;321:342–62.

[16] Malekzadeh P. Three-dimensional free vibration analysis of thick functionally graded plates on elastic foundations. Compos Struct 2009;90:428–37.

[17] Huang ZY, Lü CF, Chen WQ. Benchmark solutions for functionally graded thick plates resting on Winkler–Pasternak elastic foundations. Compos Struct 2008;85:95–104.

[18] Civalek O, Akgöz B. Non-linear vibration analysis of laminated plates resting on nonlinear two parameters elastic foundations. Steel Compos Struct 2011;11(5):403–21.

[19] Civalek O. Nonlinear analysis of thin rectangular plates on Winkler–Pasternak elastic foundations by DSC–HDQ methods. Appl Math Model 2007;31:606–24.

[20] Civalek O. Harmonic differential quadrature-finite differences coupled approaches for geometrically nonlinear static and dynamic analysis of rectangular plates on elastic foundation. J Sound Vib 2006;294:966–80.
[21] Dumir PC, Kumar CR, Gandhi ML. Non-linear axisymmetric vibration of orthotropic thin circular plates on elastic foundations. J Sound Vib 1985;103:273–85 (1985).
[22] Zhou D, Lo SH, Au FTK, Cheung YK. Three dimensional free vibration of thick circular plates on Pasternak foundation. J Sound Vib 2006;292:726–41.
[23] Hosseini Hashemi SH, Rokni Damavandi Taher H, Omidi M. 3-D free vibration analysis of annular plates on Pasternak elastic foundation via p-Ritz method. J Sound Vib 2008;311:1114–40.
[24] Malekzadeh P, Golbahar Haghighi MR, Atashi MM. Free vibration analysis of elastically supported functionally graded annular plates subjected to thermal environment. Meccanica 2011;46:893–913.
[25] Wattanasakulpong N, Ungbhakorn V. Linear and non linear vibration analysis of elastically restrained ends FGM beams with porosities. Aerosp Sci Technol 2014;32:111–20.
[26] Leissa AW. Non-linear analysis of plate and shell vibrations: proceeding of the second international conference on structural dynamics; recent advances. Southampton 1984(1):241–60.
[27] Sathyamoorthy M. Non-linear vibration analysis of plates: a review and survey of current developments. Appl Mech Rev 1987;40:1553–61.
[28] Chia CY. Non-linear analysis of plates. New York: McGraw-Hill; 1980.
[29] Chia CY. Geometrically non-linear behavior of composite plates: a review, Appl Mech
[30] Amabili M, Paidoussis MP. Review of studies on geometrically non-linear vibrations and dynamics of circular cylindrical shells and panels, with and without fluid structure interaction. Appl Mech Rev 2003;56(4):349–81 [Rev 1988;41:439–51].
[31] Aydogdu M, Taskin V. Free vibration analysis of functionally graded beams with simply supported edges. Mater Des 2007;28:1651–6.
[32] Piovan MT, Sampaio R. Vibration of axially moving flexible beams made of functionally graded materials. Thin-Walled Struct 2008;46:112–21.
[33] Xiang HJ, Yang J. Free and forced vibration of a laminated FGM Timoshenko beam of variable thickness under heat conduction. Composites: Part B 2008;39:292–303.
[34] Yang J, Shen HS. Vibration characteristics and transient response of shear-deformable functionally graded plates in thermal environment. J Sound Vib 2002;255:579–602.
[35] Qian LF, Batra RC, Chen LM. Static and dynamic deformations of thick functionally graded elastic plates by using higher-order shear and normal deformable plate theory and meshless local Petrov–Galerkin method. Composites: Part B 2004;35:685–97.
[36] Kim YW. Temperature dependent vibration analysis of functionally graded rectangular plates. J Sound Vib 2005;284:531–49.
[37] Batra RC, Jin J. Natural frequencies of a functionally graded anisotropic rectangular plate. J Sound Vib 2005;282:509–16.
[38] Chen CS, Chen TJ, Chien RD. Non-linear vibration of initially stressed functionally graded plates. Thin-Walled Struct 2006;44:844–51.
[39] Batra RC. Higher-order shear and normal deformable theory for functionally graded incompressible linear elastic plates. Thin-Walled Struct 2007;45:974–82.
[40] Gupta AK, Kumar L. Thermal effect on vibration of non-homogeneous visco-elastic rectangular plate of linearly varying thickness. Meccanica 2008;43:47–54.
[41] Gupta AK, Kaur H. Study of the effect of thermal gradient on free vibration of clamped visco-elastic rectangular plate with linearly thickness variation in both directions. Meccanica 2008;43:449–58.
[42] Zhao X, Liew KM. Geometrically nonlinear analysis of functionally graded plates using the element free kp-Ritz method. Comput Methods Appl Mech Eng 2009;198:2796–811.
[43] Reddy JN, Wang CM, Kitipornchai S. Axisymmetric bending of functionally graded circular and annular plates. Eur J Mech–A/Solids 1999;18:185–99.
[44] Gunes R, Reddy JN. Non-linear analysis of functionally graded circular plates under different loads and boundary conditions. Int J Struct Stabil Dyn 2008;8:131–59.
[45] Ma LS, Wang TJ. Non-linear bending and post-buckling of a functionally graded circular plate under mechanical and thermal loadings. Int J Solids Struct 2003;40:3311–30.
[46] Prakash T, Ganapathi M. Asymmetric flexural vibration and thermo elastic stability of FGM circular plates using finite element method. Composites: Part B 2006;37:642–9.
[47] Eraslan AN, Akis T. On the plane strain and plane stress solutions of functionally graded rotating solid shaft and solid disk problems. Acta Mech 2006;181:43–63.
[48] Efraim E, Eisenberger M. Exact vibration analysis of variable thickness thick annular isotropic and FGM plates. J Sound Vib 2007;299:720–38.
[49] Nie GJ, Zhong Z. Semi-analytical solution for three-dimensional vibration of functionally graded circular plates. Comput Methods Appl Mech Eng 2007;196:4901–10.
[50] Dong CY. Three-dimensional free vibration analysis of functionally graded annular plates using the Chebyshev–Ritz method. Mater Des 2008;29:1518–25.
[51] Nie GJ, Zhong Z. Dynamic analysis of multi-directional functionally graded annular plates. Appl Math Model 2010;34:608–16.
[52] Chakraverty S, Jindal R, Agarwal VK. Effect of non homogeneity on natural frequencies of vibration of elliptic plates. Meccanica 2007;42:585–99.
[53] Benamar R. Non-linear dynamic behaviour of fully clamped beams and rectangular isotropic and laminated plates. PhD thesis. University of Southampton; 1990. p. 35–62.
[54] Benamar R, Bennouna MMK, White RG. The effects of large vibration amplitudes on the mode shapes and natural frequencies of thin elastic structures, part I: simply supported and clamped-Clamped beams. J Sound Vib 1991;149:179–95.
[55] Benamar R, Bennouna MMK, White RG. The effects of large vibration amplitudes on the mode shapes and natural frequencies of thin elastic structures. Part II: fully clamped rectangular isotropic plates. J Sound Vib 1991;164:399–424.
[56] Benamar R, Bennouna MMK, White RG. The effects of large vibration amplitudes on the mode shapes and natural frequencies of thin elastic structures. Part III: fully clamped rectangular isotropic plates-measurement of the mode shape amplitude dependence and spatial distribution of harmonic distortion. J Sound Vib 1991;175:377–95.
[57] Moussaoui F, Benamar R, White RG. The effects of large vibration amplitudes on the mode shapes and natural frequencies of thin elastics shells. Part I: coupled transverse-circumferential mode shapes of isotropic circular cylindrical shells of infinite length. J Sound Vib 2000;232(5):917–43.
[58] Moussaoui F, Benamar R, White RG. The effects of large vibration amplitudes on the mode shapes and natural frequencies of thin elastics shells. Part II: a new approach for free transverse constrained vibration of circular cylindrical shells. J Sound Vib 2002;255:931–63.
[59] Harras B, Benamar R, White RG. Geometrically non-linear free vibration of fully clamped symmetrically laminated rectangular composite plates. J Sound Vib 2002;251(4):579–619.
[60] Harras B, Benamar R, White RG. Experimental and theoretical investigation of the linear and nonlinear dynamic behaviour of a glare 3 hybrid composite panel. J Sound Vib 2002;252(2):281–315.
[61] Azrar L, Benamar R, White RG. A semi-analytical approach to the non-linear dynamic response. Problem of S–S and C–C beams at large vibration amplitudes. Part I: general theory and

application to the single mode approach to free and forced vibration analysis. J Sound Vib 1999;224:377–95.
[62] Azrar L, Benamar R, White RG. A semi-analytical approach to the non-linear dynamic response problem of beams at large vibration amplitudes, part II: multimode approach to the forced vibration analysis. J Sound Vib 2002;255:1–41.
[63] Azrar L, Benamar R, White RG. Non-linear free and forced response of beams at large vibration amplitudes by a semi-analytical method. In Proceedings of the seventh international conference–structural dynamics. Southampton, England; 2000.
[64] El Kadiri M, Benamar R, White RG. Improvement of the semi-analytical method, for determining the geometrically non-linear response of thin straight structures. Part I: application to clamped–clamped and simply supported–clamped beams. J Sound Vib 2002;249(2):263–305.
[65] El Kadiri M, Benamar R. Improvement of the semi-analytical method, for determining the geometrically nonlinear response of thin straight structures. Part II: first and second non-linear mode shapes of fully clamped rectangular plates. J Sound Vib 2002;257:19–62.
[66] El Bikri K, Benamar R, Bennouna MM. Geometrically non-linear free vibrations of clamped simply supported rectangular plates. Part I: the effects of large vibration amplitudes on the fundamental mode shape. Comput Struct 2003;81:2029–43.
[67] El Bikri K, Benamar R, Bennouna MM. Geometrically non-linear free vibrations of clamped–clamped beams with an edge crack. Comput Struct 2006;84:485–502.
[68] Haterbouch M, Benamar R. The effects of large vibration amplitudes on the axisymmetric mode shapes and natural frequencies of clamped thin isotropic circular plates. Part I: iterative and explicit analytical solution for non-linear transverse vibrations. J Sound Vib 2003;265:123–54.
[69] Haterbouch M, Benamar R. The effects of large vibration amplitudes on the axisymmetric mode shapes and natural frequencies of clamped thin isotropic circular plates. Part II: iterative and explicit analytical solution for non-linear coupled transverse and in-plane vibrations. J Sound Vib 2004;277:1–30.
[70] Amabili M, Garziera R. A technique for the systematic choice of admissible functions in the Rayleigh–Ritz method. J Sound Vib 1999;224(3):519–39.
[71] Han W, Petyt M. Geometrically non-linear vibration analysis of thin, rectangular plates using the hierarchical finite element method–I: the fundamental mode of isotropic plates. Comput Struct 1997;63(2):295–308.
[72] Han W, Petyt M. Geometrically non-linear vibration analysis of thin, rectangular plates using the hierarchical finite element method–II: first mode of laminated plates and higher modes of isotropic and laminated plates. Comput Struct 1997;63(2):309–18.
[73] Ribeiro P. Geometrical non-linear vibration of beams and plates by the hierarchical finite element method. Ph.D. thesis. University of Southampton; 1998.
[74] Praveen GN, Reddy JN. Nonlinear transient thermo elastic analysis of functionally graded ceramic–metal plates. Int J Solids Struct 1998;35:4457–76.
[75] Wattanasakulpong N, Prusty BG, Kelly DW, Hoffman M. Free vibration analysis of layered functionally graded beams with experimental validation. Mater Des 2012;36:182–90.
[76] Reddy JN, Wang CM, Kitipornchai S. Axisymmetric bending of functionally graded circular and annular plates. Eur J Mech–A/Solids 1999;18:185–99.
[77] Reddy JN, Huang CL, Singh IR. Large deflections and large amplitude vibrations of axisymmetric circular plates. Int J Numer Meth Eng 1981;17:527–41.
[78] Chia CY. Non-linear analysis of plates. New York: McGraw-Hill; 1980.
[79] Serge Abrate. Functionally graded plates behave like homogeneous plates. Composites: Part B 2008;39:151–8.
[80] Brush DO, Almorth BO. Buckling of bars, plates and shells. New York: McGraw-Hill; 1975 [ISBN: 0904 188965].
[81] Powell MJD. A method for minimising a sum of squares of non-linear functions without calculating derivatives. Comput J 1965;7:303–7.
[82] Leissa AW. Vibration of Plates. NASA SP-160, National Aeronautics and Space Administration. Washington, DC; 1969.
[83] Vera SA, Febbo M, Rosit CA, Dolinko AE. Transverse vibrations of circular annular plates with edges elastically restrained against rotation, used in acoustic underwater transducers. Ocean Eng 2002;29:1201–8.
[84] Han JB, Liew KM. Axisymmetric free vibration of thick annular plates. Int J Mech Sci 1999;41(9):1089–109.
[85] Zhou ZH, Wong KM, Xu XS, Leung AYT. Natural vibration of circular and annular thin plates by Hamiltonian approach. J Sound Vib 2011;330:1008–17.
[86] Bashmal S, Bhat R, Rakheja S. In-plane free vibration of circular annular disks. J Sound Vib 2009;322(1–2):216–26.

Lhoucine Boutahar had obtained the Degree of Master of Mechanical Engineering. He is a professor of Mechanical Engineering and Vibration Studies at Higher School of Technical Education (ENSET) of Rabat, Mohamed V-University, MOROCCO – Associate professor at the laboratory of mechanical innovation and industrially Production (LaMIPI). He had participated in many international seminars and conferences (Mechanics of Composites NewYork USA 8–12 June 2014 – Eurodyn 2014 Porto 30 June au 02 July 2014). He has published two research papers in International Journal of Mechanical Science and Engineering, one research paper in Advanced Materials Research and one research paper in the proceedings of the 9th International Conference on Structural Dynamics, EURODYN 2014. He prepares his Ph.D on Mechanical Engineering and Vibration under the supervision of the Professors Rhali Benamar and El bikri Khalid.

Khalid El bikri is a professor on Mechanical Engineering and Vibration Studies at Higher School of Technical Education (ENSET de RABAT), Mohamed V-University, Rabat, Morocco. He is a Ph.D. degree holder on Mechanical Engineering and Vibration (2004) delivered by Mohammedia School of Engineering, Mohamed V-University, Rabat, Morocco. He is head of Mechanical Engineering Department and Coordinator of the master degree in Mechanical Engineering.

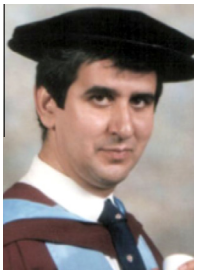

Rhali Benamar is a professor on Mechanical Engineering and Vibration Studies at Mohammedia School of Engineering, Mohamed V University, Agdal, Rabat, Morocco. He got a diploma in Civil Engineering in 1982 delivered by the Ecole National des Ponts et des Chaussées, Paris, France. He got his Ph.D., in 1990 delivered by the Institute of Sound and Vibration, University of Southampton, U.K.